

Directional Audio System

A Low Cost Implementation of A Directional Audio System



Presented by:
Dillon Alexander Heald

Prepared for:
A/Prof. A. J. Wilkinson
Dept. of Electrical and Electronics Engineering
University of Cape Town

Submitted to the Department of Electrical Engineering at the University of Cape Town in partial fulfilment of the academic requirements for a Bachelor of Science degree in Electrical and Computer Engineering.

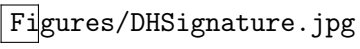
May 2020

Key words:

Directional Audio System, Directional Acoustics, Sound from Ultrasound, Parametric Acoustic Array

Declaration

1. I know that plagiarism is wrong. Plagiarism is to use another's work and pretend that it is one's own.
2. I have used the IEEE convention for citation and referencing. Each contribution to, and quotation in, this report from the work(s) of other people has been attributed, and has been cited and referenced.
3. This report is my own work.
4. I have not allowed, and will not allow, anyone to copy my work with the intention of passing it off as their own work or part thereof.

Signature:  Figures/DHSsignature.jpg

Dillon Alexander Heald

Date: 3 July 2020

Abstract

This thesis project aims develop a low cost prototype of a directional audio system based on the self-demodulating phenomenon described by Berkay's far-field solution for ultrasonic pressure waves in air as a medium. The thesis initially outlines relevant theory relating to the directionality of traditional loudspeakers and how higher directionality is achieved with ultrasonic waves. The prior works of the field are mentioned with some discussion of its relevance to the proposed prototype solution. The signal chain is simulated for better understanding of the self-demodulating phenomenon followed by various subsystem designs to implement this signal chain. These designs include mixing, amplification, pre-processing and ultrasonic array designs which are then simulated to verify their operation before their implementation. Each subsystem implementation is tested and compared to simulations with results fed back into the implemented designs to improve their outputs. The directionality and distortion testing methods are then defined and executed for the test setup. The results reveal a significant amount of distortion from the 1st harmonic of the test tone, however; a directional audio beam is achieved featuring self-demodulation. These results are then discussed to further interrogate sources of uncertainty and identify that the modulation technique implemented may be causing added distortion, particularly with the 1st harmonic. The conclusion identifies that the project successfully implemented a low-cost directional speaker and goes on to recommend future improvements for the project.

Acknowledgements

I would like to make a special thank you to my family for their continued support and encouragement throughout my undergraduate degree.

Further thanks are extended to my core friend group at UCT consisting of Jehan, Clara, Elle and Stefan who provided continued emotional support and challenging discussion from the beginning of my undergraduate degree.

Additionally, I would like to thank my significant other, Caryn; for her endless encouragement in my work and patience with me during challenging times.

Finally, I thank Associate Prof. Andrew Wilkinson for believing in my self-proposed thesis topic and working tirelessly with me through the many challenges we faced during its development.

Contents

| | |
|--------------------------------------------------------|------------|
| List of Figures | iii |
| List of Tables | vi |
| 1 Introduction | 1 |
| 1.1 Background | 1 |
| 1.2 Problem statement | 1 |
| 1.3 Project objectives | 2 |
| 1.3.1 Theory & simulation | 2 |
| 1.3.2 Design | 2 |
| 1.3.3 Implementation | 2 |
| 1.3.4 Testing & verification | 3 |
| 1.4 Scope and limitations | 3 |
| 1.5 Document outline | 4 |
| 2 Literature Review | 5 |
| 3 Theory & Simulation | 7 |
| 3.1 Signal generation | 7 |
| 3.2 Pre-processing | 7 |
| 3.3 Environment transfer function simulation | 9 |
| 3.4 Simulation results and discussion | 11 |
| 3.4.1 Pre-processing | 11 |
| 3.4.2 Environment transfer function | 13 |
| 3.5 Simulation complications | 16 |
| 4 Design | 17 |
| 4.1 High level system design | 17 |
| 4.2 Pre-processing subsystem design | 17 |
| 4.3 Mixer design | 18 |
| 4.3.1 Mixer simulations | 19 |
| 4.4 Amplifier design | 21 |
| 4.4.1 Amplifier simulations | 22 |
| 4.5 Ultrasonic array design | 24 |
| 4.5.1 Element packing | 24 |
| 4.5.2 Array design simulations | 28 |
| 4.5.3 Array PCB design | 33 |
| 5 Implementation | 37 |

| | | |
|----------|--------------------------------------------------------------------------------------|-----------|
| 5.1 | Circuit construction | 37 |
| 5.1.1 | AD633 Linear amplitude modulator implementation | 37 |
| 5.1.2 | Amplifier Implementation | 38 |
| 5.2 | Transducer array construction | 41 |
| 5.3 | Pre-processing development | 43 |
| 6 | Testing Methodology | 44 |
| 6.1 | Test setup and apparatus | 44 |
| 6.2 | Distortion testing method | 45 |
| 6.3 | Directionality testing method | 46 |
| 7 | Results | 47 |
| 7.1 | Distortion testing | 47 |
| 7.1.1 | Traditional loudspeaker distortion results | 47 |
| 7.1.2 | Square-root AM versus AM ultrasonic directional speaker distortion results | 48 |
| 7.2 | Directivity testing | 49 |
| 7.2.1 | Directivity of a traditional loudspeaker | 49 |
| 7.2.2 | Directivity of the directional audio system | 52 |
| 8 | Discussion & Conclusion | 55 |
| 8.1 | Discussion | 55 |
| 8.2 | Conclusion | 57 |
| 8.3 | Future improvements | 58 |
| 9 | References | 59 |
| A | Audio pre-processing code | 61 |
| B | Project management & planning | 63 |
| B.1 | Work breakdown structure | 63 |
| B.2 | Gantt chart | 64 |
| C | Beam pattern simulation code | 67 |

List of Figures

| | | |
|-----|----------------------------------------------------------------------------------------------------------------------------------------------------------------------------------------------------------------------------------|----|
| 2.1 | Functional diagram created by Gan et al. demonstrating primary and resulting secondary beams created from a parametric acoustic array | 6 |
| 2.2 | Simulated comparison between conventional and parametric loudspeakers created by Gan et al. | 6 |
| 3.1 | The time domain representation of the 1 kHz signal after the first and second integral | 11 |
| 3.2 | The frequency domain representation of the 1 kHz signal after the first and second integral | 11 |
| 3.3 | The frequency domain representation of the 1 kHz double integrated and square rooted signal followed by its amplitude modulation with a 40 kHz carrier wave . | 12 |
| 3.4 | The frequency domain representation of the 1 kHz signal after squaring done by medium, overlayed with the FIR filter shape and the result of the filter's application. | 13 |
| 3.5 | The frequency domain representation of the 1 kHz signal after squaring done by medium but with amplification for better representation, overlayed with the FIR filter shape and the result of the filter's application. | 13 |
| 3.6 | The frequency domain representation of the received 1 kHz signal without amplification after squaring and filtering magnified between 0 and 2.5 kHz . | 14 |
| 3.7 | The frequency domain representation of the 1 kHz signal after first and then second derivatives | 14 |
| 3.8 | The time domain representation of the 1 kHz signal after first and then second derivatives (blue) compared to a scaled representation of the original 1kHz function (orange) | 15 |
| 3.9 | The time domain representation of the 1 kHz signal after passing through the environmental transfer function simulator (blue) being blocked out by a sample for sample match with the original 1 kHz function (orange) | 15 |
| 4.1 | High level system design for the directional audio system | 17 |
| 4.2 | Signal pre-processing flowchart | 18 |
| 4.3 | AD633 functional diagram | 18 |
| 4.4 | LTS spice circuit for AD633 Linear Amplitude Modulator | 19 |
| 4.5 | Input and output voltage of the AD633 based linear amplitude modulator (V_{in} at 1V amplitude) | 20 |
| 4.6 | Input and output voltage of the AD633 with V_{in} at 1.95V amplitude demonstrating ideal modulation index | 20 |
| 4.7 | Input and output voltage of the AD633 with V_{in} at 2.5V amplitude demonstrating over-modulation | 20 |
| 4.8 | Input and output voltage of the AD633 with V_{in} at 1.75V amplitude | 21 |

| | | |
|------|------------------------------------------------------------------------------------------------------------------------------|----|
| 4.9 | The circuit design adapted from phono amplifier example application within LM380 datasheet | 21 |
| 4.10 | Input voltage versus output voltage of the LM380 at 40 kHz | 22 |
| 4.11 | Output voltage on the output pin of the LM380 at 40 kHz | 22 |
| 4.12 | Output voltage on the output pin of the LM380 compared to supply voltage . . | 23 |
| 4.13 | Output voltage on the output pin of the LM380 compared to supply voltage with a reduced peak-to-peak input voltage | 23 |
| 4.14 | Output current of the LM380 through the simulated ultrasonic transducer array | 24 |
| 4.15 | Densest possible pattern in a circle of radius 4.1cm | 25 |
| 4.16 | Densest density information for a circle of radius 4.1cm | 25 |
| 4.17 | Rectangular packing pattern in a circle of radius 4.1cm | 25 |
| 4.18 | Density information with square packing for a circle of radius 4.1cm | 25 |
| 4.19 | Hexagonal packing pattern in a circle of radius 4.1cm | 26 |
| 4.20 | Density information with hexagonal packing for a circle of radius 4.1cm . . | 26 |
| 4.21 | Densest packing pattern in a circle of radius 4.5cm | 26 |
| 4.22 | Density information with densest packing for a circle of radius 4.5cm . . . | 26 |
| 4.23 | Hexagonal packing pattern in a circle of radius 4.5cm | 27 |
| 4.24 | Density information with hexagonal packing for a circle of radius 4.5cm . . | 27 |
| 4.25 | Square packing pattern in a circle of radius 4.5cm | 27 |
| 4.26 | Density information with square packing for a circle of radius 4.5cm . . . | 27 |
| 4.27 | Single ultrasonic transducer element to be modeled | 29 |
| 4.28 | Approximate beam shape of a single ultrasonic transducer (Bore-sight view) . | 29 |
| 4.29 | Approximate beam shape of a single ultrasonic transducer (3D view) | 30 |
| 4.30 | Square packed ultrasonic transducer elements to be modeled | 30 |
| 4.31 | Approximate beam shape of the square packed ultrasonic transducer array (Bore-sight view) | 30 |
| 4.32 | Approximate beam shape of square packed ultrasonic transducer array (3D view) | 31 |
| 4.33 | Hexagonally packed ultrasonic transducer elements to be modeled | 31 |
| 4.34 | Approximate beam shape of the hexagonally packed ultrasonic transducer array (Bore-sight view) | 31 |
| 4.35 | Approximate beam shape of hexagonally packed ultrasonic transducer array (3D view) with scale | 32 |
| 4.36 | Approximate beam shape of hexagonally packed ultrasonic transducer array (3D shifted view to display sidelobes) | 32 |
| 4.37 | Rev 1.0 illustrating a modular octagonal design | 33 |
| 4.38 | Rev 1.1 illustrating a modular hexagonal design with extra pin headers . . . | 34 |
| 4.39 | Three Rev 1.1 modular hexagonal PCBs interconnecting | 35 |
| 4.40 | Rev 1.2 monolithic design derived from packing simulations | 36 |
| 4.41 | Isometric 3D view of Rev 1.2 Circular PCB design with square packing . . . | 36 |

| | | |
|------|---------------------------------------------------------------------------------------------------------------------------------------------------------|----|
| 4.42 | bottom 3D view of Rev 1.2 Circular PCB design with square packing | 36 |
| 5.1 | AM mixer implemented on breadboard | 37 |
| 5.2 | Input 2.5 kHz frequency compared to modulated output | 38 |
| 5.3 | Input 40 kHz frequency compared to modulated output | 38 |
| 5.4 | AM mixer output versus input signal | 38 |
| 5.5 | LM380 Power amplifier breadboard circuit after troubleshooting | 39 |
| 5.6 | LM380 Power amplifier circuit schematic after troubleshooting | 39 |
| 5.7 | LM380 Power amplifier 500 Hz output to test speaker | 40 |
| 5.8 | Front side of unpopulated PCB | 41 |
| 5.9 | Back side of unpopulated PCB | 41 |
| 5.10 | Front side of populated PCB | 41 |
| 5.11 | Back side of populated PCB | 41 |
| 5.12 | Transducer emitting in-phase output | 42 |
| 5.13 | Transducer emitting out of phase output | 42 |
| 5.14 | Time domain representation of original tone and output pre-processed tone . . | 43 |
| 5.15 | Frequency domain representation of original tone and output pre-processed tone | 43 |
| 6.1 | The test setup used for distortion and directionality testing. | 45 |
| 7.1 | The spectrum and time domain signal of the traditional loudspeaker with a 2.5kHz input tone | 47 |
| 7.2 | The positive spectrum of the traditional loudspeaker with a 2.5kHz input tone . | 47 |
| 7.3 | The spectrum and time domain signal of the square root amplitude modulated ultrasonic speaker with a 2.5kHz input tone | 48 |
| 7.4 | The positive spectrum of the square root amplitude modulated ultrasonic speaker with a 2.5kHz input tone | 48 |
| 7.5 | The spectrum and time domain signal of the amplitude modulated ultrasonic speaker with a 2.5kHz input tone | 48 |
| 7.6 | The positive spectrum of the amplitude modulated ultrasonic speaker with a 2.5kHz input tone | 48 |
| 7.7 | The spectrum and time domain signal of the square root amplitude modulated ultrasonic speaker (microphone outside of beam) with a 2.5kHz input tone . . | 49 |
| 7.8 | The positive spectrum of the square root amplitude modulated ultrasonic speaker (microphone outside of beam) with a 2.5kHz input tone | 49 |
| 7.9 | Original beam sweep recording and FFT of all samples for traditional loudspeaker | 49 |
| 7.10 | Filtered 2.5kHz time domain signal emitted from a traditional speaker over beam sweep | 50 |
| 7.11 | Filtered 2.5kHz spectrum emitted from a traditional speaker over beam sweep . | 50 |
| 7.12 | Filtered 5kHz time domain signal emitted from a traditional speaker over beam sweep | 51 |
| 7.13 | Filtered 5kHz spectrum emitted from a traditional speaker over beam sweep . | 51 |

| | | |
|------|------------------------------------------------------------------------------------------------------------|----|
| 7.14 | Filtered 7.5kHz time domain signal emitted from a traditional speaker over beam sweep | 51 |
| 7.15 | Filtered 7.5kHz spectrum emitted from a traditional speaker over beam sweep | 51 |
| 7.16 | Original beam sweep recording and FFT of all samples for a ultrasonic directional speaker | 52 |
| 7.17 | Filtered 2.5kHz time domain signal emitted from a ultrasonic directional speaker over beam sweep | 52 |
| 7.18 | Filtered 2.5kHz spectrum emitted from a ultrasonic directional speaker over beam sweep | 52 |
| 7.19 | Filtered 5kHz time domain signal emitted from a ultrasonic directional speaker over beam sweep | 53 |
| 7.20 | Filtered 5kHz spectrum emitted from a ultrasonic directional speaker over beam sweep | 53 |
| 7.21 | Filtered 7.5kHz time domain signal emitted from a ultrasonic directional speaker over beam sweep | 54 |
| 7.22 | Filtered 7.5kHz spectrum emitted from a ultrasonic directional speaker over beam sweep | 54 |
| B.1 | Work breakdown structure for the the directional audio system | 64 |
| B.2 | Gantt chart part 1 | 64 |
| B.3 | Gantt chart part 2 | 65 |
| B.4 | Gantt chart part 3 | 65 |
| B.5 | Gantt chart part 4 | 66 |

List of Tables

| | | |
|---|--------------------------------------------------|----|
| I | Table of apparatus used during testing | 44 |
|---|--------------------------------------------------|----|

1 Introduction

1.1 Background

Audible sound for human hearing lies between 20 to 20kHz and classical speakers perform well at achieving a natural response to match this. However, classical speakers cannot easily control where the sound waves go and instead fill the space that the loudspeaker occupies uniformly. This is due to the large wavelength of audible sound which limits the maximum directivity of a loudspeaker.

Directivity for a sound source is related to the ratio of wavelength (λ) to the aperture diameter ($D_{aperture}$) of the source as shown in equation 1 and results in a beam angle. Note, however; this equation is only true for small beam angles.

$$B_\theta \approx \frac{\lambda}{D_{aperture}} \quad (1)$$

For apertures much larger than the wavelengths it produces, a high directivity is achieved. Since audible sound has a wavelength between 17 meters to 1.7 centimetres, an infeasible aperture diameter would be required to achieve a high directivity.

If instead the transmitted waves are ultrasound, the wavelengths are reduced to between 5.7 to 8.5 millimetres allowing for a smaller aperture of a few centimetres to achieve a high directivity.

1.2 Problem statement

Since these ultrasonic waves are inaudible, they need to be translated down in frequency to the human hearing range. This can be done by exploiting a property of air acting as a nonlinear medium when propagating ultrasonic waves. According to Berkay's far-field solution [1], the secondary pressure wave is proportional to the second time derivative of the primary pressure wave squared. A simplified form of Berkay's far-field solution ignoring medium related constants is shown in equation 2 where $p_1(t)$ and $p_2(t)$ represent the primary (input) and secondary (output) sound pressure waves respectively when an ultrasonic wave is propagated in a medium.

$$p_2(t) \propto \frac{\partial^2}{\partial t^2} p_1^2(t) \quad (2)$$

The non-linearity caused by the squaring shown in equation 2 creates sum and difference frequencies when sinusoidal waves are applied. Since the sinusoidal waves are in the ultrasonic range, the sum produces higher ultrasonic frequencies while the difference produces lower audible baseband frequencies.

This translation from ultrasonic to audible frequencies is known as self-demodulation and causes the ultrasonic beam itself to become a virtual loudspeaker which extends the aperture diameter beyond the physical bounds of the radiating transducers, thus improving directivity of the audible sound.

1.3 Project objectives

This thesis project aims to produce a simple, low-cost prototype of the above mentioned directional audio system to demonstrate the directional audio effect which can be further refined in future revisions.

The deliverables involved in the development of the directional audio system are broken up into developmental milestones which feed into one another and are discussed in the following subsections.

1.3.1 Theory & simulation

The theory deliverable involves understanding the various models related to the development of the directional audio system. This includes understanding the principles behind self-demodulating ultrasonic waves and how to implement these principles.

The principles understood in theory must then be tested by simulation where the full signal path is simulated from generation/recording, pre-processing of the signals and finally to recreation of the medium within which the ultrasonic waves are produced. The simulations will deliver a flexible environment to test pre-processing ideas and modulation schemes within some simulation limits. Additionally, the simulations aid in providing a flexible development environment to implement pre-processing of signals for the physical implementation while maintaining a low cost.

1.3.2 Design

This deliverable aims to create designs and simulations of the multiple subsystems required to produce the directional audio system. These subsystems include an ultrasonic transducer array, audio signal pre-processing subsystem, modulation circuit and ultrasonic signal amplifier. Each of these designs may need to be iterated upon, thus prototyping and testing of these subsystems during their development is expected.

1.3.3 Implementation

The implementation of the selected designs for each subsystem involves construction of each subsystem followed by subsystem level testing where the subsystems are given controlled inputs and their outputs are measured and evaluated. The results from these tests may require changes to the original designs or alterations to the expected outputs of each subsystem to align with what is feasibly possible in the physical implementation.

1.3.4 Testing & verification

The testing and verification of the directional audio system will be done by comparing its acoustic performance with a traditional loudspeaker of similar aperture diameter. Particular test points of interest include the directionality of the speaker and the audible harmonic distortion for the pure tone case. The results will be captured by microphone recording in an appropriate test environment. The recordings will then be processed to extract spectrum information for harmonic distortion investigation and a representation of the directionality of both systems.

1.4 Scope and limitations

The constraints of the directional audio system involve both complexity limitations based on the allocated time frame of the project and developmental limitations due to circumstances external to the projects control.

The complexity scope limitation constrains the analytical depth the project may go into in favour of having a functional deliverable by the end of the project. The allotted time for the project spans an academic semester where the final deliverable is this document reporting on the simulation, design, implementation and testing of the directional audio system. Additionally a poster summarising the document is required.

These limitations also include a budget of less than ZAR 1500 which reduces the achievable scope of the project to a low-cost solution as wide bandwidth transducers and high performance DSPs are outside of this budget and cannot be loaned for its duration.

External factors from the project also limit the scope by changing the work environment during development. This project was undertaken in the first semester of 2020, midway through this semester the Covid-19 pandemic struck the world and resulted in a national lockdown; thus restricting access to lab resources at UCT. Fortunately some basic lab equipment remained accessible and could be used at home during the national lockdown.

1.5 Document outline

The report segments into seven sections (excluding the introduction) which each feature one of the developmental milestones from the previously introduced project objectives as well as a brief literature review and conclusion. These sections are listed below along with a summarised introduction to what is discussed in each section.

- Section 2 walks through the history of the phenomenon and how it has evolved through the years. Results and advancements in the technology related to the phenomenon are mentioned and cited.
- Section 3 describes the simulation of the related signals for the directional audio system while relating it to the theory it represents. Each stage in the signal chain is described in theory and simulated. Measurements on this signal chain are performed with different signal processing factors to ascertain how these factors might effect the time and frequency domain of the signal as it passes through the simulated system.
- Section 4 elaborates on the designs needed to implement the simulated signal chain for the directional audio system. The subsystems include some high level system designs, electrical designs and transducer array designs. Each design is simulated to confirm its output aligns with what it is designed to achieve. Heavier emphasis is put into the transducer array design including element packing and beam shape simulations.
- Section 5 depicts the physical implementation of each designed subsystem. Tests at subsystem level for each implemented design are carried out with relevant conclusions drawn for moving forward with the implemented design.
- Section 6 specifies the testing method used to test the distortion and directionality of a traditional loud speaker system compared to the directional audio system. The test setup is defined, test methods are described and result generation methods outlined.
- Section 7 presents the results gathered from the distortion and directionality testing described in section 6. The results are described and points of interest are mentioned.
- Section 8 discusses the results from section 7, drawing conclusions relating to the distortion and directionality of the directional audio system. The project as a whole is then concluded, with particular retrospective points of interest mentioned. The section ends off with further improvements for the project being discussed.

2 Literature Review

Creating lower frequency waves from higher frequency waves by non-linear interaction began in the field of sonar through development of underwater sonar techniques as far back as the 1960's in a publication by Westervelt [2]. These developments produced a formal mathematical basis for the effect of directive ultrasonic transducers arrays and were referred to as parametric arrays.

While these sonar systems were developed for underwater use, a publication in 1975 by the Acoustical Society of America [3] revealed that the nonlinear effects observed underwater could occur in air as well.

By 1983, companies such as Ricoh [4] developed directional loudspeaker systems; however, found them quite costly to consider as a viable product for exhibits and museum installations. Their implementations were rudimentary with basic equalisation of the audio signal and double side band amplitude modulation. They identified a proportional relationship between the modulation depth (m) and the sound pressure of the signal; however, found that the distortion is proportional to m^2 .

By 1998, Kite [5] proved that the distortion can be reduced by preprocessing this signal appropriately. Pompei [6] implemented the square root amplitude modulation (SRAM) technique proposed by Kite which overcame the squaring of the envelope signal first identified by Berkay's approximation. This reduced the harmonic distortion compared to Double Side Band Amplitude Modulation (DSBAM) used before.

Kite [5] noted that the distortion can be totally removed if the harmonics of the modulating signal created by the square root process in SRAM are reproduced by the ultrasonic transducers themselves. However, this would require an infinite bandwidth in the ideal case or atleast more than 10 kHz of bandwidth for each transducer in the array which was found to be infeasible.

The past innovations in the field neglected to consider the bandwidth of the transducers themselves. In 2009, Tan et al. [7] tackled this problem by considering a different modulation approach using Modified Amplitude Modulation (MAM). This modulation scheme involved a form of quadrature amplitude modulation which took into account the 3dB bandwidth of the transducers themselves. This further lowered the distortion present in the demodulated signal. By 2012, Gan et al. [8] reviews the existing techniques in the directional audio phenomenon with a glimpse into new related works. During this review the theoretical framework of parametric acoustic arrays is discussed where primary and secondary beams are described as a result of fundamental and difference frequency components. The secondary source column of the difference frequency creates a virtual secondary beam within the primary beam as shown in the figure created by Gan et al. re-presented in figure 2.1 [8]. A practical demonstration of the directionality phenomenon is shown through simulation and is reiterated in figure 2.2 [8] where a single element speaker is compared to a parametric speaker (with matching 10cm

radius) producing an audible 2 kHz tone from its secondary beam using an ultrasonic 40 kHz primary beam.

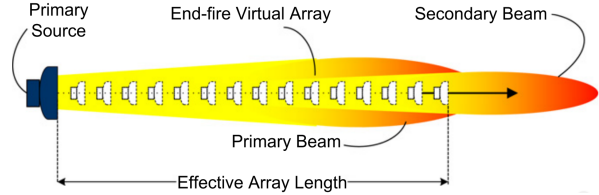


Figure 2.1: Functional diagram created by Gan et al. demonstrating primary and resulting secondary beams created from a parametric acoustic array.

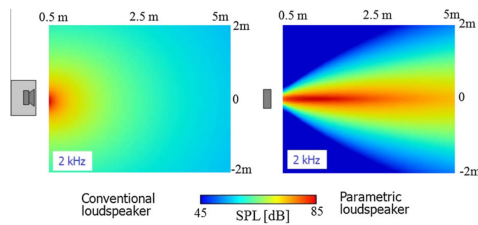


Figure 2.2: Simulated comparison between conventional and parametric loudspeakers created by Gan et al.

Recent studies suggest that the harmonic distortion is related to the frequency response of the ultrasonic transducers not being considered in Berklay's equation; however, a paper from 2018 [9] suggests this can be overcome by choosing a suitable modulation technique and applying a filter which describes the transducer array's frequency response.

In terms of real world applications of directional audio systems, Dr. Pompei went on to further develop his directional Audio Spotlight at the MIT Media Lab during his Ph.D. and founded Holosonics to commercialise the technology. This resulted in the technology finding application in museums and galleries, digital signage, libraries, hospitals and retail settings [10]. In review of the major prior works done in the field of directional acoustics; progress towards a viable directional audio system is feasible in both commercial and academic settings. While a lot of the techniques used by these prior works show great promise for a high quality directional audio system, they make little mention of the costs involved in producing such a system since their focus is on perfecting their individual techniques. Holosonic's products show commercial feasibility of this system but have price ranges of between \$500 to \$2000 and as a result are not low cost implementations. The directional audio system discussed in this report aims to produce a low cost implementation with the potential to be further iterated on to improve its quality in the future. This low cost implementation will likely be far more rudimentary than these systems given the previously mentioned scope and limitations of the project, thus cannot be directly compared to the outputs of the above mentioned works. Rather, the techniques used in these prior works will be implemented where possible and explored to identify a middle ground between a feasible, low cost implementation and a quality directional audio output device.

3 Theory & Simulation

The purpose of the simulations were to identify what the main signal processing factors are when producing a directional audio system. To do so, the audible signal had to be generated, passed through the inverse transfer function of the environment defined by Berklay's approximation shown in equation 2 and finally applied to the approximate transfer function of the environment along with appropriate filtering to mimic the human hearing range. The outcome from these simulations would show what factors were important in the synthesis of a directional ultrasonic beam and the audible demodulation of said beam. All signal simulations were done in Julia [11] with aid from the FFTW [12] Julia standard libraries.

3.1 Signal generation

During initial simulations a 1kHz tone denoted by $x(t)$ and a carrier signal at 40kHz defined as $x_{cw}(t)$ were generated. $x(t)$ was chosen to be a sine wave while $x_{cw}(t)$ was set as a cosine function to simplify the mathematics involved. Both signals were then passed into the signal pre-processing stage of the simulation.

$$x(t) = \sin(\omega_0 t) \quad (3)$$

$$x_{cw}(t) = \cos(\omega_c t) \quad (4)$$

The 1kHz tone and carrier signal are denoted by ω_0 and ω_c respectively.

3.2 Pre-processing

To achieve an audible signal in the environment, the inverse function of the environment must be applied to the signal prior to transmission. Berklay's approximation [1] shown in equation 2, has the following inverse shown below in equation 5.

$$p_{out}(t) = \iint \sqrt{p_1(t)} dt^2 \quad (5)$$

$p_1(t)$ represents the pressure wave to be heard in the environment. By applying the second time integral to the square root of the original waveform, the environment will apply its second time derivative to the square of the output function ($p_{out}(t)$) resulting in the original audible pressure waves as shown below in equation 6 and 7.

$$p_2(t) \approx \frac{\partial^2}{\partial t^2} \left(\iint \sqrt{p_1(t)} dt^2 \right)^2 \quad (6)$$

$$p_2(t) \approx p_1(t) \quad (7)$$

Implementing this type of signal processing in the simulation was done on a discrete sample by sample level to allow for easier adaptability of any processing factors that may arise. The double integration of the signal was done by use of a simple left sided Riemann sum shown in listing 1. For each result, the input signals value is multiplied by sample period (Δt) and then added to the previous result of the integral. Edge cases were handled by starting at the second sample and assuming the integral starts at the origin.

Listing 1: Left sided integration function written in Julia

```
function integrate(x, Δt)
    y=zeros(length(x));
    N = length(x)
    for n=2:N
        y[n]=x[n-1]*Δt + y[n-1]
    end
    return y
end
```

With each integration, the mean of the signal is subtracted from the the original signal to correct the signal back to the origin as shown in listing 2. This shift is necessary as the drift in signal level limits its ability to be produced out of a real transducer.

Listing 2: Shifting signal to its average value before integration

```
#Pre-process signal
y'=integrate(x.-mean(x),Δt)      #perform first integral of the audio signal
y''=integrate(y'.-mean(y'),Δt)    #perform second integral of the audio signal
```

Following the integration steps, the absolute value of the signal is determined and the square root applied, shown in listing 3. The absolute value is necessary as the square root of the negative samples would yield an imaginary result which cannot practically be reproduced in the real world implementation. The signal is finally modulated with a 40kHz carrier wave for transmission into the simulated medium.

Listing 3: Take absolute value of integrated signal and apply the square root

```
y'' = y''.-minimum(y'')           #shifts the signal to above 0
yout = y''.^^(1/2)                 #Square root the signal
yout_mod = yout.*x_carrier        #Modulate the preprocessed signal with carrier
```

3.3 Environment transfer function simulation

The pre-processed signal is now applied to the environment's transfer function by applying the mathematical operations shown in equation 2. The first operation which is applied is the squaring of the pre-processed signal. This is done by taking the square of each sample with the use of the power operator in Julia. This squared signal is then transformed to its Fourier transformed representation so a FIR filter can be applied. The filter construction is shown in listing 4 and forms a tophat function from -15kHz to 15kHz to filter out any signals outside of the band of human hearing.

Listing 4: FIR filter for mimicing human hearing

```

Δω = 2*pi/(N*Δt) # Sample spacing in freq domain in rad/s
ω = 0:Δω:(N-1)*Δω # Define angular frequency
B = 30000 # filter bandwidth of 30KHz to span from -15 to 15 KHz
H = rect.(ω/(2*pi*B)) + rect.((ω .- 2*pi/Δt)/(2*pi*B)) #Tophat = _|----|_
Hs=[i[1] for i in H]# Change array type so ifft works

#transform function into frequency domain
YOUT_sqr = fft(yout_mod_sqr)
#Apply filter
YOUT_sqr_LPF = YOUT_sqr.*Hs

```

Application of the filter is done by multiplying the Fourier representations of the filter with the signal shown in the lower portion of listing 4.

The signal is then transformed back into the time domain for the last stage of signal processing. The double time derivative of the time domain expression is then applied to account for the $\frac{\partial}{\partial t}$ of equation 2. Additionally the time domain expression is multiplied by 2 to account for the halving of the signal when taking only the real parts of a inverse Fourier transform. Listing 7 shows the implementation of the inverse Fourier transform and double derivatives in Julia. The `deriv()` function is defined in listing 5 which applies a left sided derivative to each sample much like the integral defined in listing 1.

Listing 5: derivative function implementing a sample wise left sided derivative

```

function deriv(x,Δt)
    y=zeros(length(x))
    N = length(x)
    for n=2:N
        y[n]=(x[n]-x[n-1])/Δt
    end
    return y
end

```

The `shiftBackBy()` function is a function which shifts a sampled signal back by a number of samples. Its purpose is to remove the artifacts that occur during the sample wise differentiation. These artifacts occur due to the initial value of the signal being set to 0 during differentiation. A shift of a single sample would not be noticeable to human hearing and thus should not be considered an issue for the system as a whole. The code for this shifting function is shown in listing 6

Listing 6: Function for shifting sampled signal back by a set number of samples

```
function yshift=shiftBackBy(x,shift)
    yshift=zeros(length(x))
    N = length(x)
    for n=1:N-shift
        yshift[n]=x[n+shift]
    end
    return yshift
end
```

Listing 7: Conversion to time domain and double time derivative

```
yout_mod_sqr_lpf = 2*real(ifft(YOUT_sqr_LPF))    #Extract  time-domain

yout_mod_sqr_dt1_lpf = deriv(yout_mod_sqr_lpf,Δt)  #Differentiate signal once
yout_mod_sqr_dt1_lpf = shiftBackBy(yout_mod_sqr_dt1_lpf,1)
yout_mod_sqr_dt2 = deriv(yout_mod_sqr_dt1_lpf,Δt)  #Differentiate signal again
yout_mod_sqr_dt2 = shiftBackBy(yout_mod_sqr_dt2,1)
```

The final signal `yout_mod_sqr_dt2` is the time domain expression of the audio signal after it has passed through the environment simulation.

3.4 Simulation results and discussion

The results for major parts in the signal chain from the simulations will be presented here and discussed.

3.4.1 Pre-processing

During pre-processing, the signal undergoes a double integral. The time domain representation of the signal after the first and second integrals is shown in figure 3.1. The positive frequency domain representation of the first and second integral are shown in figure 3.2.

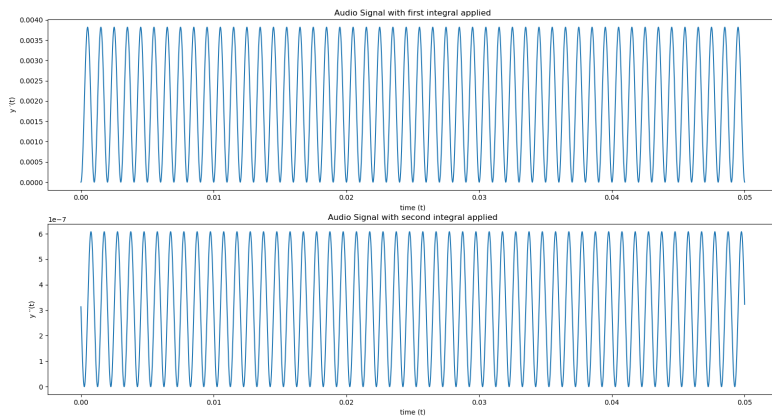


Figure 3.1: The time domain representation of the 1 kHz signal after the first and second integral

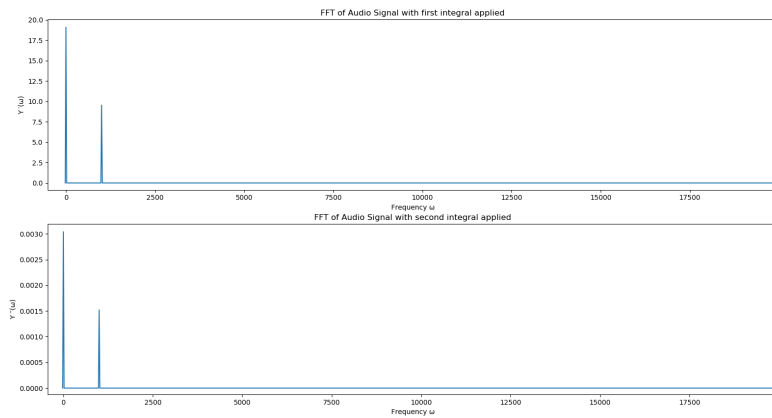


Figure 3.2: The frequency domain representation of the 1 kHz signal after the first and second integral

The only notable difference between these results is the decrease in amplitude of the sine wave as well as a phase shift of about 90° between the time domain representations in figure 3.1. This phase shift is expected since the integral of a sinusoidal function produces another sinusoidal function with a phase shift.

Moving forward within the pre-processing chain, the result of these integrals is then square-rooted according to the code shown in listing 3. This results in decaying harmonics as shown in figure 3.3 which are then modulated with the 40 kHz carrier signal through AM modulation. The spectrums in figure 3.3 show a large fundamental component with

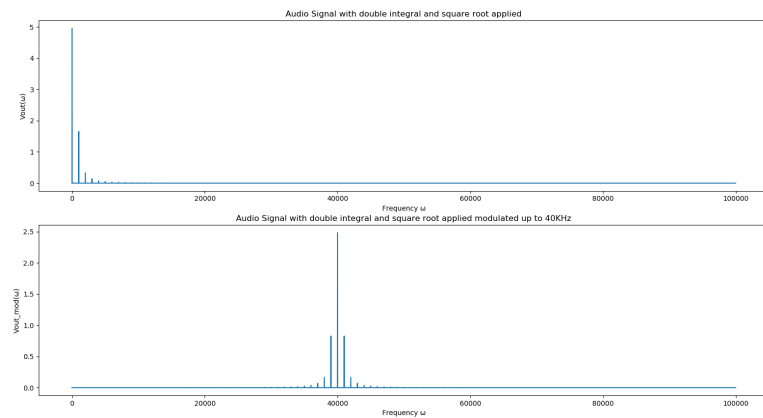


Figure 3.3: The frequency domain representation of the 1 kHz double integrated and square rooted signal followed by its amplitude modulation with a 40 kHz carrier wave

exponentially decaying harmonics. The fundamental along with its harmonics is then shifted up to 40 kHz without any aliasing. This result assumes that the bandwidth of the transducers are infinite and as such, are able to replicate all of these harmonics, however; this is not the case in practice. The bandwidth of the ultrasonic transducers is constrained to 2.5 kHz in the practical implementation since larger bandwidth transducers are impractical for a low cost implementation. This will result in imperfect inverse reproduction of the original signal when applied to the environment and likely result in deteriorated signal quality after demodulation.

3.4.2 Environment transfer function

The output of the pre-processing simulation results in our processed signal modulated up to 40kHz. The environment then applies the mathematical operations from equation 2 which starts with the squaring of the signal. Figure 3.4 shows the result of squaring the modulated output (Y_{OUT}) from the pre-processing simulation as well as the FIR filter described in listing 4 along with the result from applying this filter. The result of the squaring of the signal is not immediately apparent and has been artificially amplified in figure 3.5 to demonstrate where the frequency components of the signal now lie.

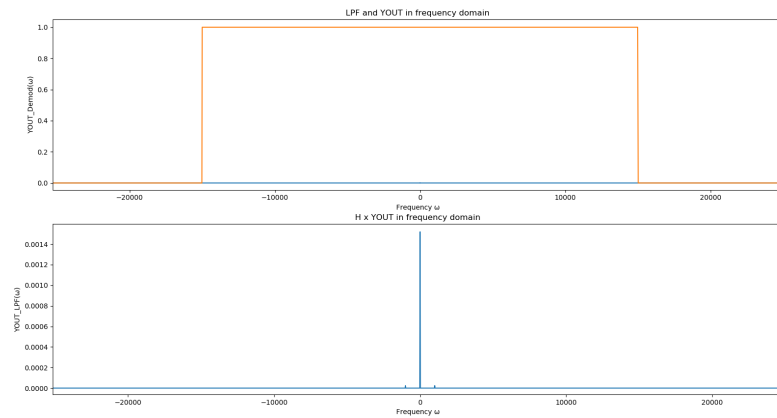


Figure 3.4: The frequency domain representation of the 1 kHz signal after squaring done by medium, overlaid with the FIR filter shape and the result of the filter's application.

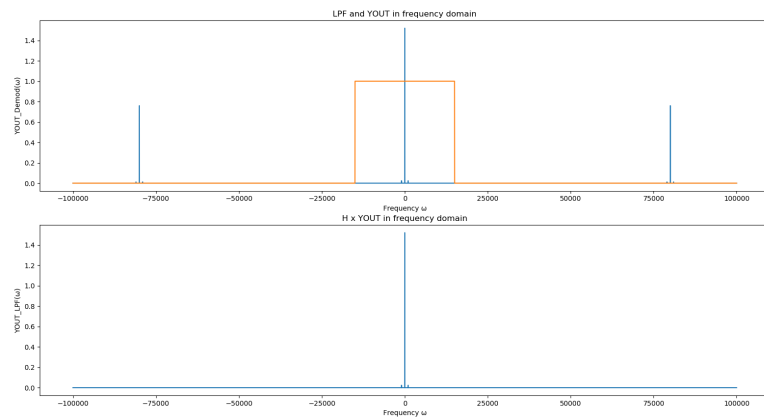


Figure 3.5: The frequency domain representation of the 1 kHz signal after squaring done by medium but with amplification for better representation, overlaid with the FIR filter shape and the result of the filter's application.

The amplified signal in figure 3.5 shows sum and difference frequencies at 80 kHz and baseband respectively. Upon application of the filter, only baseband signals are shown. A closer look at the baseband spectrum is shown in figure 3.6 which represents a strong low frequency component with very small 1 kHz components.

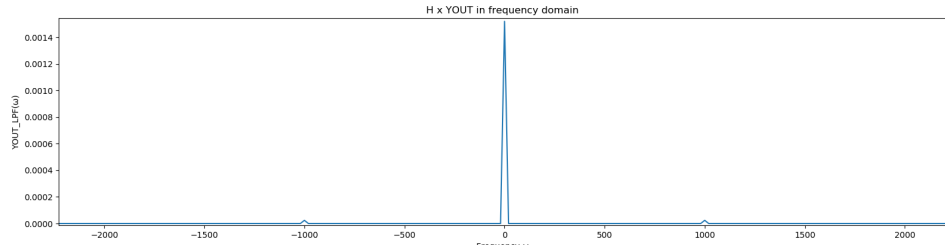


Figure 3.6: The frequency domain representation of the received 1 kHz signal without amplification after squaring and filtering magnified between 0 and 2.5 kHz

The next function the environment applies to the signal is a double derivative as described in listing 5. The results from the first and second derivative are shown in figure 3.7. The derivatives appear to amplify the low amplitude 1kHz components while effectively cancelling out the low frequency baseband signal acquired from the difference pair in the squaring process. By the application of the second derivative, the relative magnitude of the signal is significantly stronger.

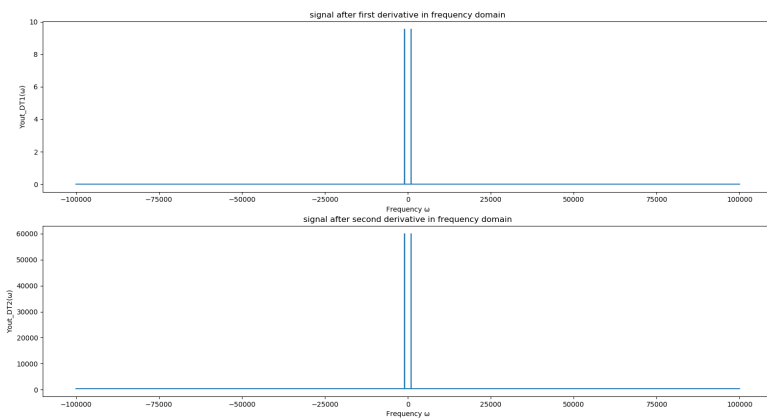


Figure 3.7: The frequency domain representation of the 1 kHz signal after first and then second derivatives

The time domain representations of each derivative is compared to the original 1 kHz signal in figure 3.8 where the output of the first and second derivatives are in blue and the original signal (scaled for easier comparison) is in orange. Notably, the signal after the first derivative

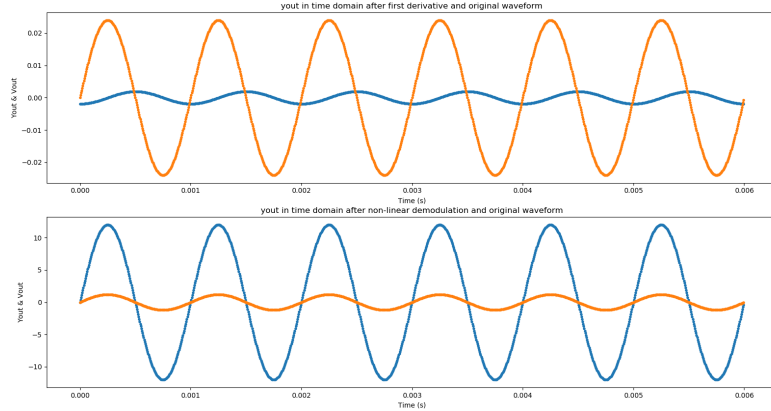


Figure 3.8: The time domain representation of the 1 kHz signal after first and then second derivatives (blue) compared to a scaled representation of the original 1kHz function (orange)

is out of phase with the original by 90° . However; after the second derivative the phases match. This is expected behaviour since the derivative of a sinusoidal function is that function again, shifted in phase by 90° .

Finally, to analyse the sample by sample representation of the output; figure 3.9 is plotted without any modification to the original signals amplitude nor phase.

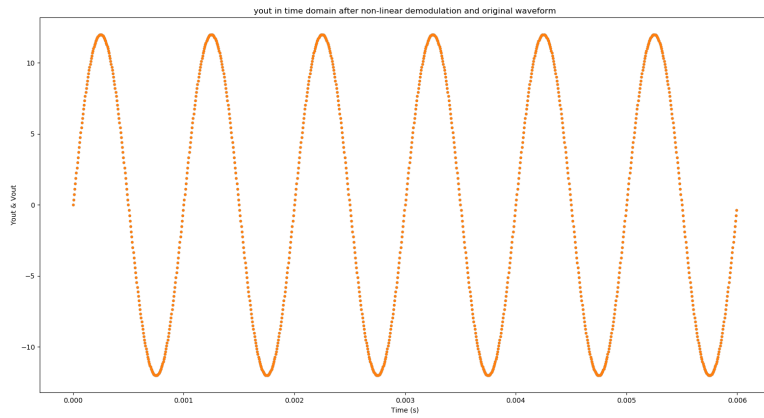


Figure 3.9: The time domain representation of the 1 kHz signal after passing through the environmental transfer function simulator (blue) being blocked out by a sample for sample match with the original 1 kHz function (orange)

Upon inspection, a sample for sample match of the input and output sinusoidal signals is achieved, thus blocking out the demodulated signals samples (blue) with the original functions samples (orange). This result demonstrates the full signal simulation was successful and all mathematical operations applied by the simulated environment were overcome with pre-processing.

While this result is expected in the theory and simulation, it remains unknown how the bandwidth limitations of the transducers will effect the output. The ultrasonic transducer's transfer function is not modelled nor is its frequency response as this is left to be a potential future improvement of the simulation for a future iteration of this project. This future iteration of the simulation might consider measuring the frequency response of the transducers and using this data to apply a filter to the 40 kHz AM output signal.

3.5 Simulation complications

During the initial implementation of the signal pre-processing and environment modelling stages, the discrete signal processing outputs were causing artefacts in the signal plots. This was caused by the `deriv()` functions in code listings 5. The outputs of the derive function were discontinuous because the first sample of the input signal ($x[n-1]$ where n is 1) is 0 while the second sample of the input signal ($x[n-1]$ where n is 2) is a much larger number than 0. This discontinuity caused a large spike in the output of the function between the first two samples. Initially this was discovered by setting $y[1]=y[2]$ which yielded the correct output for a derivative of the input function. Later it was decided that the first sample of our signal did not really hold much value due to the high number of samples in the sampled signal and the `shiftBackBy()` function was created to shift the signal back by a sample and thus, remove that first sample from the output.

4 Design

The design of the directional audio system involves many individual subsystems to achieve the directional audio beam. This section breaks down and describes the design of each of these subsystems.

4.1 High level system design

The high level system design of the directional audio system is shown in figure 4.1 where the flows between each component are illustrated. The system begins by pre-processing

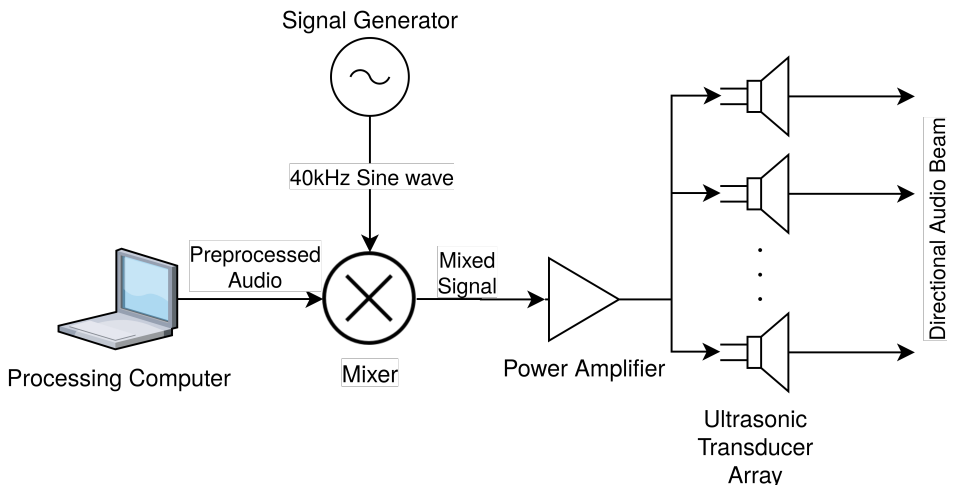


Figure 4.1: High level system design for the directional audio system

audio using a specially developed Julia program which applies the appropriate mathematical functions to a baseband audio clip and outputs the signal through the laptops audio jack. This pre-processed signal is then mixed with a 40 kHz sine wave created by a signal generator and passed into an amplifier. The amplifier increases the voltage swing of the mixed signal while having sufficient current to drive the ultrasonic transducers.

The ultrasonic transducers are connected in parallel with each other and thus all receive the same signal from the power amplifier. The transducers are packed into a densely packed array to provide a more uniform transducer aperture which emits the input signal into the environment.

4.2 Pre-processing subsystem design

The pre-processing occurs in the form of a Julia program which applies the mathematical functions shown in figure 4.2. The program takes in a sampled signal $x_{in}(t)$ which is then shifted to the centre crossing by subtraction of its average value. The function then undertakes a sample wise double integral and is then raised above the centre crossing so only positive

values remain. The square root of the function is then taken and the signal is then output through the audio port of the laptop.

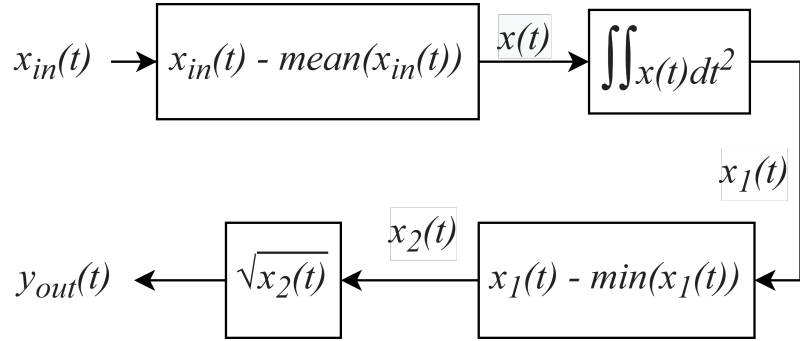


Figure 4.2: Signal pre-processing flowchart

4.3 Mixer design

The purpose of the mixer is to produce an amplitude modulated output of the carrier wave signal and the pre-processed audio signal. This can be done quite easily with the AD633 analogue multiplier with low cost supporting circuitry using the linear amplitude modulator circuit from the AD633 datasheet. The AD633 has the internal functional configuration shown in figure 4.3 where X and Y are multiplied and the result is produced on output W.

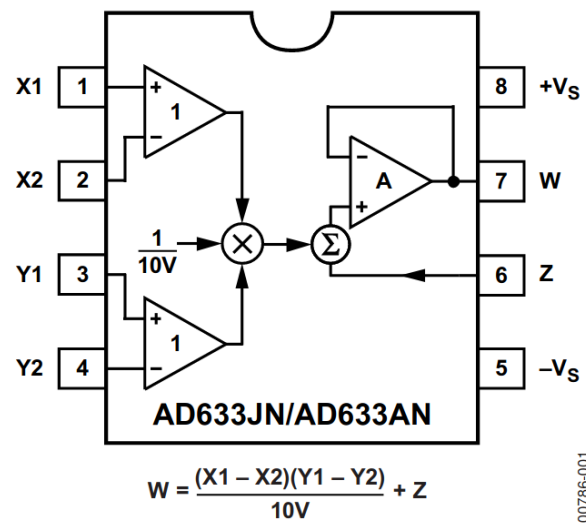


Figure 4.3: AD633 functional diagram

Analogue devices has a SPICE description of this components which was imported into LTSpice and used in the circuit shown in figure 4.4. The circuit is an implementation of the linear amplitude modulator reference circuit found in the AD633 datasheet and was adapted with relevant signal inputs (Vin, Vcarrier) to simulate the AD633's output (Vout).

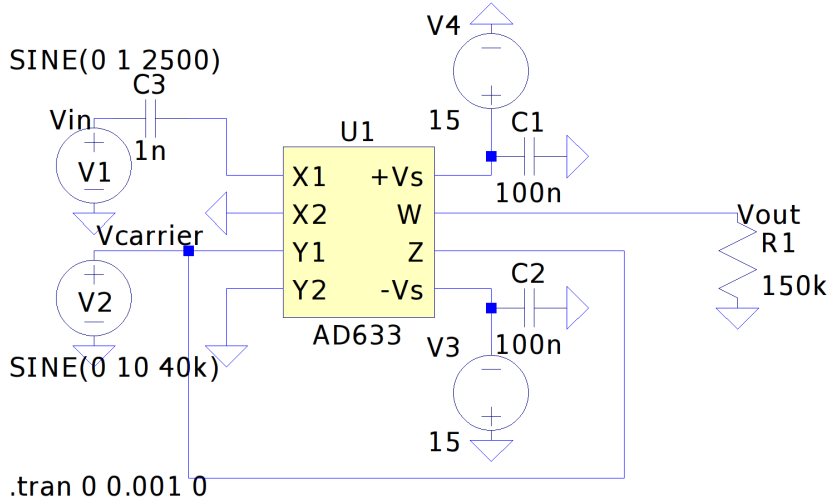


Figure 4.4: LTSpice circuit for AD633 Linear Amplitude Modulator

4.3.1 Mixer simulations

To verify the design works as intended with the systems input signals, a 40 kHz carrier with a 10V amplitude is connected to the Y input while a 2.5 kHz test tone is connected through a decoupling capacitor to the X input. The output (W) is connected to a 150k resistor to simulate the expected load of the amplifier input. The expected functional result of this configuration is shown in equation 8. Since X2 and Y2 are grounded (0V) they fall away and a double side band large carrier amplitude modulation function is the result.

$$W = \frac{(V_{in})(V_{carrier})}{10} + V_{carrier} \quad (8)$$

Figure 4.5 demonstrates the time domain expression for the output voltage across R1 as well as the input voltage V_{in} . The modulating amplitude is 1V and the carrier amplitude is 10V which are ten times the value presented to the internal multiplier as shown in figure 4.3. The simulation reveals that the output has a maximum amplitude of 2.9V and a minimum amplitude of 1.1V. This output does not produce an ideal modulation index of 100% which would produce a stronger signal strength.

To achieve a modulation index closer to 100%, the input voltage of the modulation signal would have to be increased. To illustrate this effect, the amplitude of V_{in} was adjusted until the peak voltage of the negative half cycle of the output is as close as feasibly possible to the zero crossing. Figure 4.6 demonstrates V_{in} set to a amplitude of 1.95V which achieves a lower voltage of 50mV. This is very close to the zero crossing and risks causing over-modulation if the input voltage spikes. The result of the input amplitude raising above 1.95V is shown in figure 4.7 where the input amplitude is set to 2.5V and results in the outputs' negative half-cycle peaking at 500mV which is the result of over-modulation.

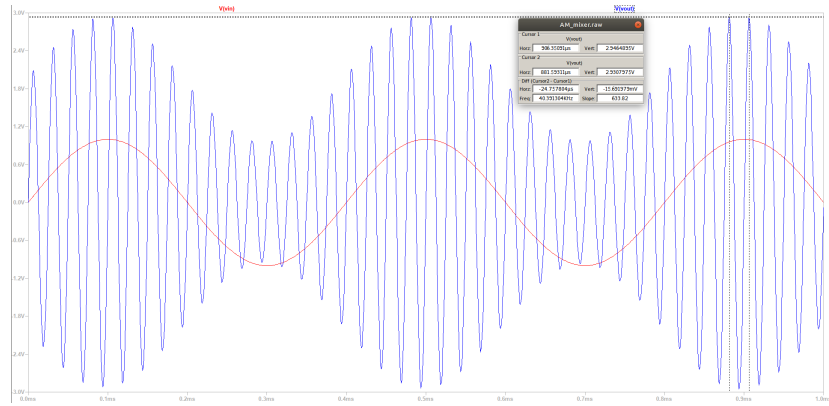


Figure 4.5: Input and output voltage of the AD633 based linear amplitude modulator (V_{in} at 1V amplitude)

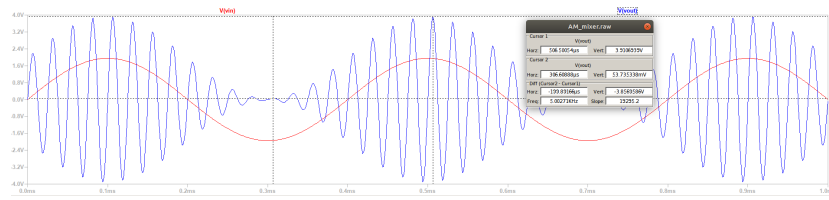


Figure 4.6: Input and output voltage of the AD633 with V_{in} at 1.95V amplitude demonstrating ideal modulation index

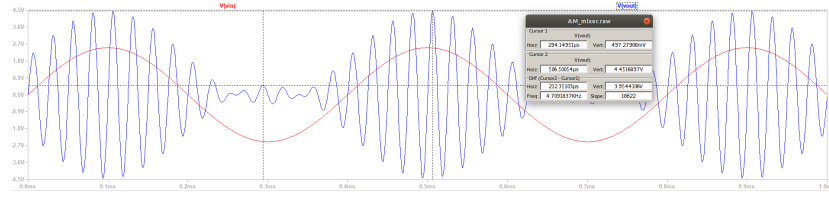


Figure 4.7: Input and output voltage of the AD633 with V_{in} at 2.5V amplitude demonstrating over-modulation

To achieve a modulation index close to 100% without risking over-modulation, the input amplitude is set to 1.75V as shown in figure 4.8. The resulting output reaches a minimum amplitude of 245mV with a maximum amplitude of 3.70V. Since the output amplitude without a modulating signal is 2V ($A_{Carrier}$), the modulation index can be calculated with equation 9 and results in an approximate modulation index of 85%.

$$m = \frac{A_{Env_peak}}{A_{Carrier}} - 1 \quad (9)$$

While a modulation index of 85% would be ideal, it is not attainable since the maximum amplitude the laptop's audio output can reach is limited to 1V. Given the prior maximum of 2.95V shown in figure 4.5, this limitation produces an approximate maximum modulation index of 48%.

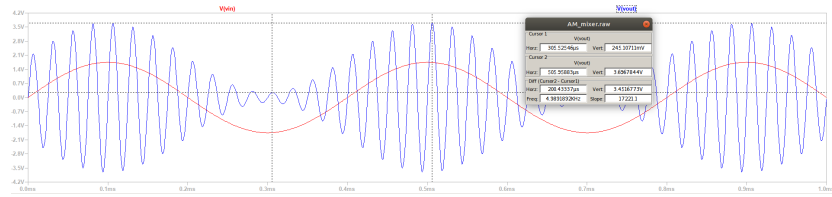


Figure 4.8: Input and output voltage of the AD633 with V_{in} at 1.75V amplitude

4.4 Amplifier design

The amplifier's purpose in the system is to increase the peak-to-peak voltage of the output signal for the ultrasonic transducers while providing sufficient current to the transducers. During existing amplifier research the Texas Instruments LM380 was chosen. Main aspects about this audio power amplifier that drove this decision included the wide supply voltage range of up to 22V, 2.5W output power and flat gain curve with a bandwidth of 100 kHz. Since the device is expected to operate around 40 kHz, the amplifier needs to respond linearly at this frequency.

The supporting circuitry for this amplifier was adapted from the phono amplifier example application circuit within the LM380's datasheet and simulated in LTSpice XVII.

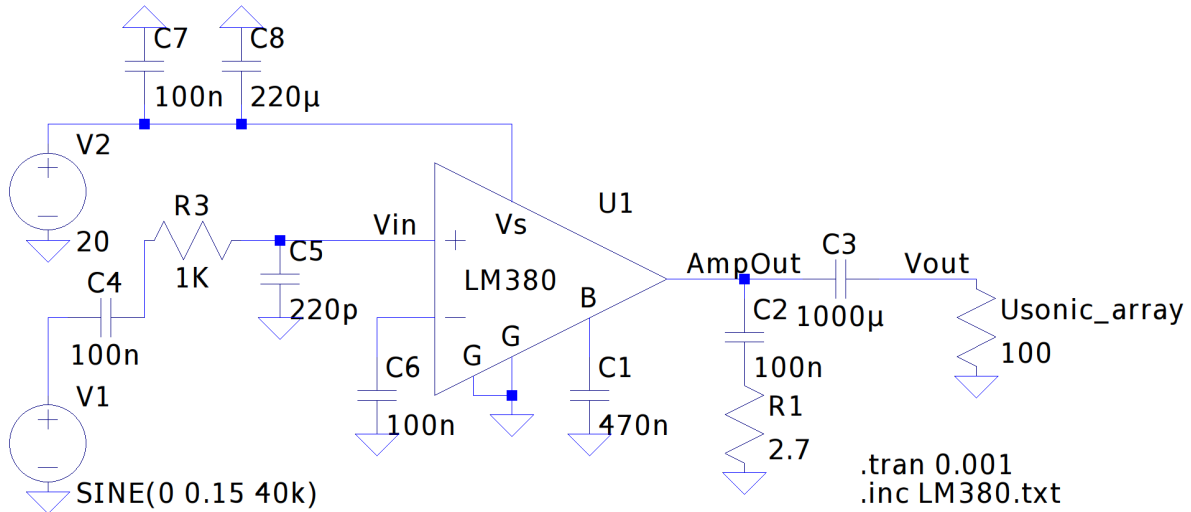


Figure 4.9: The circuit design adapted from phono amplifier example application within LM380 datasheet

Figure 4.9 shows the LM380 amplifier along with the recommended circuitry for stable operation. An assumption was made to represent the ultrasonic array as a $100\ \Omega$ resistor as from investigating the datasheet of a ultrasonic transducer, a single transducer was found to have a equivalent resistance of 1000Ω at 40 kHz. When connecting 10 of these transducers in parallel the resistance is estimated to reduce to $100\ \Omega$, hence the load in figure 4.9. If the transducer count for the array were increased to 20, this load would half down to 50Ω and

would consume approximately double the power.

4.4.1 Amplifier simulations

To verify whether the circuit in figure 4.9 would achieve the desired gain and operate at the intended carrier frequency of 40 kHz, simulations were done to test the input to output voltage (gain) as well as the output current of the LM380.

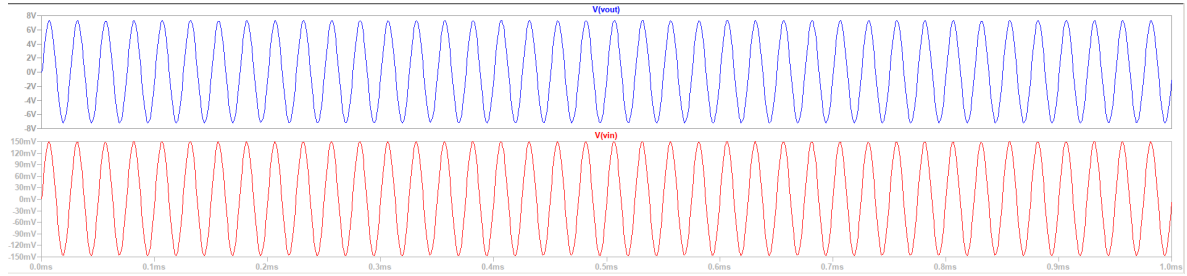


Figure 4.10: Input voltage versus output voltage of the LM380 at 40 kHz

Figure 4.10 shows the input voltage to the LM380 and the output voltage across the ultrasonic transducer array. The input voltage is $300mV_{p-p}$ while the output across the transducers is $14V_{p-p}$, resulting in a voltage gain of 46.7. Note however that this output is passed through a decoupling capacitor to centre it on the zero crossing. To investigate the upper limit of the peak-to-peak voltage swing, a measurement is made before the decoupling capacitor and the reading is shown in figure 4.11.

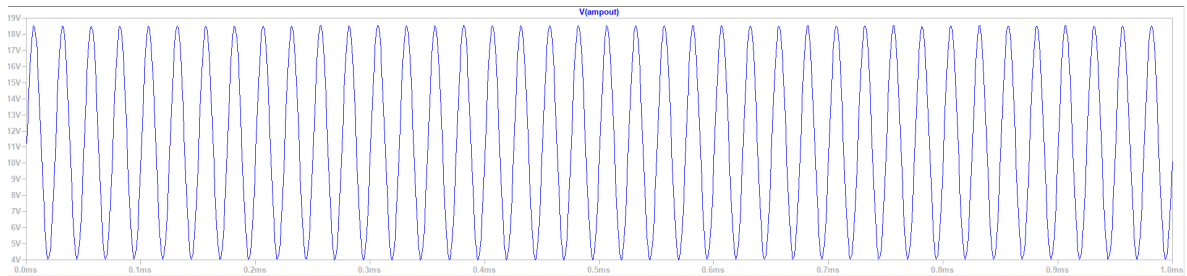


Figure 4.11: Output voltage on the output pin of the LM380 at 40 kHz

From figure 4.11 one can see the output voltage swings between 4V and 18.5V with a supply voltage of 20V. The LM380 is rated for a maximum output voltage swing of $14V_{p-p}$ and as a result it is expected the supply voltage should not go lower than 15V since that would result in the output hitting the rails of the supply and produce added noise and clipping. To test this assumption, a decreasing supply voltage was simulated to reduce the supply voltage from 20V to 15V. Figure 4.12 demonstrates the simulated relationship between supply voltage and the resultant output voltage swing of the LM380 amplifier.

The simulation reveals that there needs to be at least 6V more than the 14V peak to peak

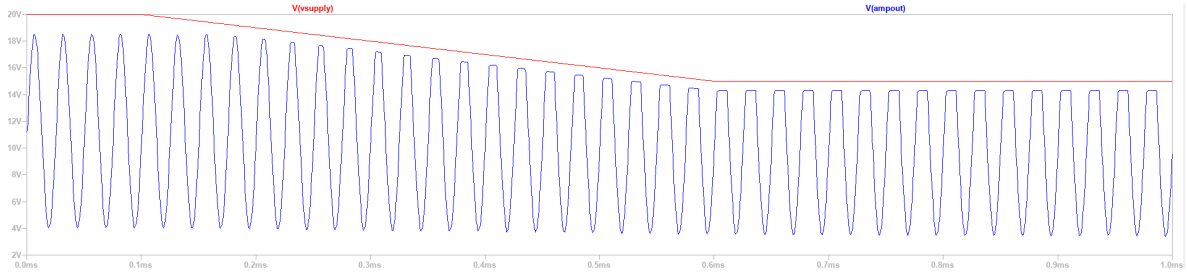


Figure 4.12: Output voltage on the output pin of the LM380 compared to supply voltage

output swing to achieve an undistorted output waveform with an input voltage of $300mV_{p-p}$. This means the supply voltage for the LM380 should remain at 20V to mitigate this clipping effect. Alternatively if the input peak-to-peak voltage is reduced to $200mV_{p-p}$ this could reduce the required supply voltage. A simulation of reducing the input voltage to $200mV_{p-p}$ is shown in figure 4.13.

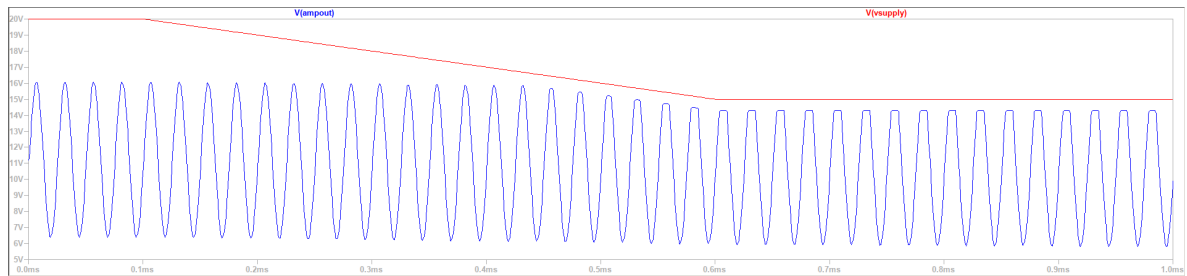


Figure 4.13: Output voltage on the output pin of the LM380 compared to supply voltage with a reduced peak-to-peak input voltage

The results of reducing the input voltage show that the LM380 amplifier can indeed operate at a lower voltage without clipping its output, however; this is due to a reduced peak-to-peak output voltage of $10V_{p-p}$. This results in a overall voltage gain of the amplifier of 50 which is larger than before, but it also reduces the peak-to-peak voltage at the output which is directly proportional to transducer movement and thus, results in a sound pressure level in the environment.

Finally the output current was simulated by measuring the current passing through the simulated ultrasonic load. Figure 4.14 demonstrates a peak-to-peak current of 140mA while producing a $14V_{p-p}$ voltage across the ultrasonic load. This results in a total power of 1.39W through the load when using RMS voltage and current in the calculation which is well within the 2.5W maximum power the LM380 is rated for. If the load were to reduce due to more transducers being added in parallel, the consumed power would increase. As long as the peak-to-peak current remains below 252mA, the amplifier is operating within the specification of its datasheet. This current translates to a load of approximately 55Ω which results in a parallel transducer configuration of 19 to 21 transducers.

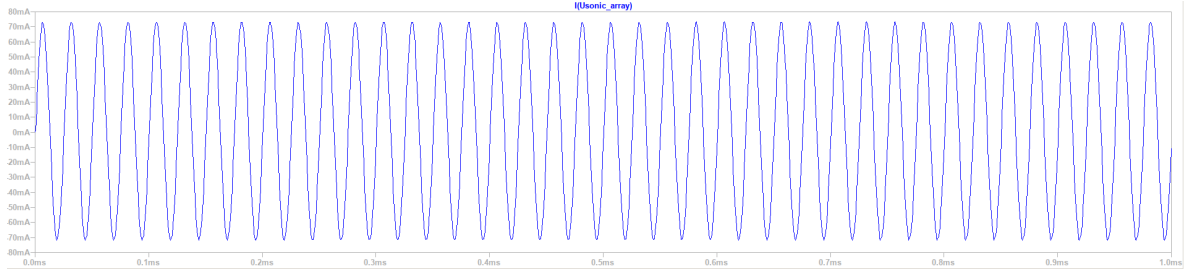


Figure 4.14: Output current of the LM380 through the simulated ultrasonic transducer array

4.5 Ultrasonic array design

The design of the directional speaker's ultrasonic array involves packing the transducers as densely as possible while maintaining a relatively circular aperture to ensure a uniform beam shape.

4.5.1 Element packing

To maximise the directivity of the ultrasonic array, the distance between the centroids of all the neighbouring transducers must be minimised. This forms a more densely packed element array and thus, a more uniform beam shape. To maximise the density of the transducers, a class of optimisation called packing can be used. The aim of packing is to insert geometric shapes in a container as densely as possible.

To evaluate possible transducer packing designs, a packing tool provided by Wolfram Alpha for 2D geometric packing [13] is used. The tool allows for dimension definition of the container (object to contain the packed geometry) as well as the packing elements (objects to be packed in the container). The container is set to varying dimensions while keeping the packing elements radius at 0.8cm as specified by the transducer's datasheet.

Packing consists of many different methods involving a particular type of symmetry. As shown in figure 4.15, a circular container with radius of 4.1cm can be packed with 20 transducers (with radius 0.8cm) producing a 76.15% filled fraction. While this may appear viable, the imbalanced placement of the transducers will produce an inconsistent beam shape resulting in a single stronger side lobe on one side of the aperture.

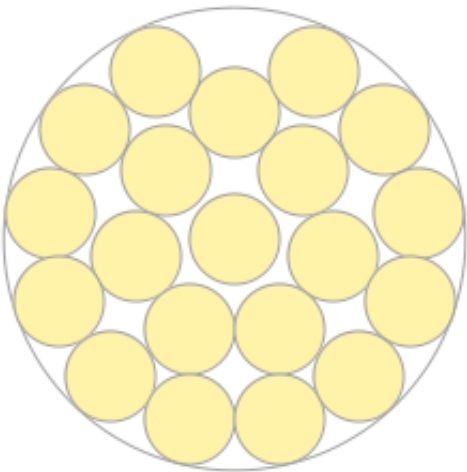


Figure 4.15: Densest possible pattern in a circle of radius 4.1cm

| | |
|------------------|----------------------|
| number | 20 |
| radius | 0.8 cm (centimeters) |
| container radius | 4.1 cm (centimeters) |
| filled fraction | 76.15% |
| empty fraction | 23.85% |
| symmetry | mirror |

Figure 4.16: Densest density information for a circle of radius 4.1cm

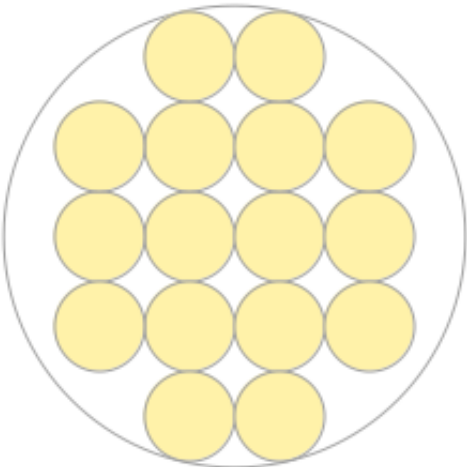


Figure 4.17: Rectangular packing pattern in a circle of radius 4.1cm

| | |
|------------------|----------------------|
| number | 16 |
| radius | 0.8 cm (centimeters) |
| container radius | 4.1 cm (centimeters) |
| filled fraction | 60.92% |
| empty fraction | 39.08% |
| symmetry | rectangular |

Figure 4.18: Density information with square packing for a circle of radius 4.1cm

Investigating an alternative type of symmetry revealed the rectangular packed result in figure 4.17. This suffers from having a lower filled fraction of 60.92% using the same 4.1cm container radius as before but shows more uniformity in transducer placement.

Another form of symmetry called inversion is investigated in figure 4.19 using the 4.1cm container radius. This configuration results in a hexagonally packed transducer placement pattern and has a filled fraction of 72.34%. The pattern allows for 19 transducers to fit within the container while maintaining even spacing between the transducers. This would result in a more uniform beam shape than the packing used in figure 4.15 as the distance between the transducers is minimised on all sides.

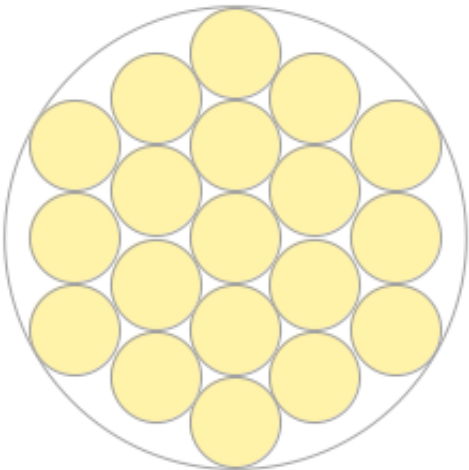


Figure 4.19: Hexagonal packing pattern in a circle of radius 4.1cm

| | |
|------------------|----------------------|
| number | 19 |
| radius | 0.8 cm (centimeters) |
| container radius | 4.1 cm (centimeters) |
| filled fraction | 72.34% |
| empty fraction | 27.66% |
| symmetry | inversion |

Figure 4.20: Density information with hexagonal packing for a circle of radius 4.1cm

To see the effect of increased container size, the container was increased slightly to a radius of 4.5cm. Unfortunately this results in erratic placement of transducers for the mirror and inversion symmetry types shown in figures 4.21 and 4.23 respectively which is undesirable for producing a uniform beam shape. The container size increase did however produce a favourable result for the square packed symmetry shown in figure 4.25, featuring a filled fraction of 66.37% with uniform placement of transducers.

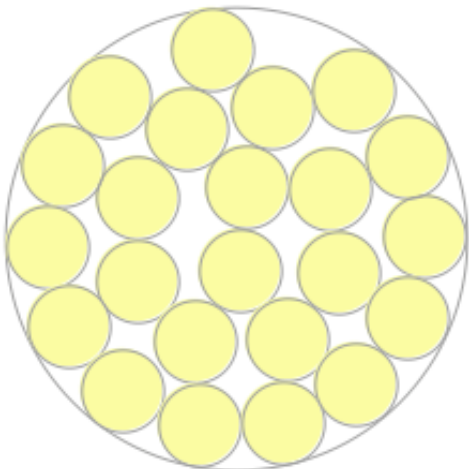


Figure 4.21: Densest packing pattern in a circle of radius 4.5cm

| | |
|------------------|----------------------|
| number | 23 |
| radius | 0.8 cm (centimeters) |
| container radius | 4.5 cm (centimeters) |
| filled fraction | 72.69% |
| empty fraction | 27.31% |
| symmetry | none |

Figure 4.22: Density information with densest packing for a circle of radius 4.5cm

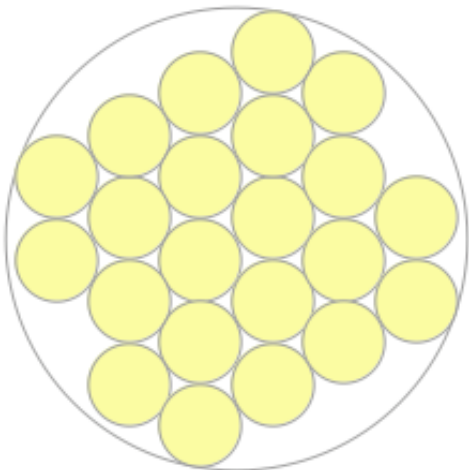


Figure 4.23: Hexagonal packing pattern in a circle of radius 4.5cm

| | |
|------------------|----------------------|
| number | 22 |
| radius | 0.8 cm (centimeters) |
| container radius | 4.5 cm (centimeters) |
| filled fraction | 69.53% |
| empty fraction | 30.47% |
| symmetry | none |

Figure 4.24: Density information with hexagonal packing for a circle of radius 4.5cm

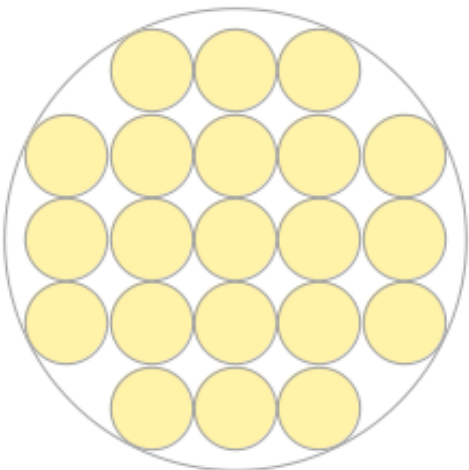


Figure 4.25: Square packing pattern in a circle of radius 4.5cm

| | |
|------------------|----------------------|
| number | 21 |
| radius | 0.8 cm (centimeters) |
| container radius | 4.5 cm (centimeters) |
| filled fraction | 66.37% |
| empty fraction | 33.63% |
| symmetry | square |

Figure 4.26: Density information with square packing for a circle of radius 4.5cm

In conclusion, two of these layouts show potential. For a container radius of 4.1cm, the hexagonally packed array shown in figure 4.19 is most effective due to its high filled fraction of 72.34% resulting in closer spacing of transducers. It does however only contain 19 transducers which is near the upper limit of the amplifier's output power but risks producing a lower output sound pressure level than a higher transducer count solution would achieve. By increasing the radius to 4.5cm, a higher transducer count of 21 is achieved in the square packed solution shown in figure 4.25 albeit with a lower filled fraction of 66.37%. The additional output power potential of the 4.5cm radius square packed array is more appealing for this application as the audible sound produced by these transducers is significantly low, thus maximising the output power of the array is a favourable design choice.

4.5.2 Array design simulations

The purpose of creating the ultrasonic array is to maximise the directivity of the speaker system. To aid in choosing an appropriate array packing profile, some designs were simulated to illustrate the effect that transducer placement in an array has on the radiated beam shape with the goal of reducing the amount of side lobes as well as their relative magnitude to the main lobe while maximising the main lobe.

The transducer patterns from figure 4.19 with hexagonal packing and figure 4.25 with square packing were simulated and compared as their designs have symmetry which is required for a uniform beam pattern.

These beam shape simulations were done by use of a two-dimensional Fourier Transform (2DFFT). The 2DFFT is performed over the parametric array aperture and forms an approximate radiated beam shape which can be used to determine how transducer placement effects the main and side lobe shapes. The beam shape simulations do not have real world axes dimensions as their intended purpose is purely for design investigation. A/Prof Wilkinson's antenna theory lecture notes [14] describe how a one dimensional FFT of a radiating aperture can be used to approximate the beam pattern of said aperture. The derivation is summarised in the following section.

FFT Beam pattern derivation: The beam pattern of a radiating aperture can be constructed by use of a two-dimensional FFT over the radiating aperture. This is done by modelling the radiating aperture as a grid of radiating point sources where the main lobe is developed from the constructive interference and side lobes created from destructive interference of these point sources, thus creating an interference pattern. This results in the waves adding in phase along the boresight axis due to constructive interference, while phase delays at some angle off boresight cause destructive interference, creating side lobes. This angle is represented by the beam width equation shown in equation 10 where D is the aperture diameter and λ is the wavelength of the waves being propagated. Note, this equation is only for small angles.

$$\theta \approx \frac{\lambda}{D} \quad (10)$$

Letting the signal received by the middle element be $\frac{Ae^{j\omega t}}{R}$ where R is the radial distance from the aperture and A is the field strength of the aperture. A can be represented as $A(x)$ which describes the field strength as a function of position away from the boresight axis. This function in the total signal received at a point being delayed by the extra distance it must travel from the transducer to the point in question. This forms a triangle with the boresight axis, x axis and ray along which the signal must travel. This distance causes a delay defined by: $\tau = \frac{x\sin(\theta)}{c}$ derived from $\Delta = xsin(\theta)$ (since $v = \frac{\Delta x}{\Delta t}$, $\Delta t = \frac{\Delta x}{v}$).

This results in the total signal received being described by equation 11.

$$E \propto \frac{1}{R} \left(\sum_n A_n e^{-j\omega\tau_n} \right) e^{-j\omega t} \quad (11)$$

Computing this sum results in an integral equation shown in equation 12.

$$E(\theta) = \frac{1}{R} \int_{x=-\infty}^{\infty} A(x) e^{j\omega(t - \frac{x \sin(\theta)}{c})} dx \quad (12)$$

Since $\frac{\omega}{c} = \frac{2\pi f}{c} = \frac{2\pi}{\lambda}$ one can rewrite the above equation as shown in equation 13

$$E(\theta) = \frac{1}{R} \int_{x=-\infty}^{\infty} A(x) e^{-j(\frac{2\pi \sin(\theta)}{\lambda})x} e^{j\omega t} dx \quad (13)$$

This angle dependant integral is in the form of a Fourier transform, thus can be computed with an FFT. Working in two dimensions allows a 3D beam pattern to be produced by performing the FFT along both dimensions. The FFT however, works with the ω axis which must be translated to an angular axis represented by θ . This can be done by the relation $\omega = \frac{2\pi \sin(\theta)}{\lambda}$, when rearranged to find θ produces $\theta = \sin^{-1}(\frac{\omega \lambda}{2\pi})$. Substituting the frequency variable $f = \frac{\omega}{2\pi}$ produces $\theta = \sin^{-1}(f\lambda)$. Appendix C demonstrates how this axis change is possible for a future implementation of this code, but does not implement it.

Single element simulation: To start, a single transducer is modelled and its approximate beam shape simulated to verify the functionality of the simulation output. The simulation output produces the expected beam pattern for a single uniform aperture in figures 4.28 and 4.29 and thus, is considered functional.

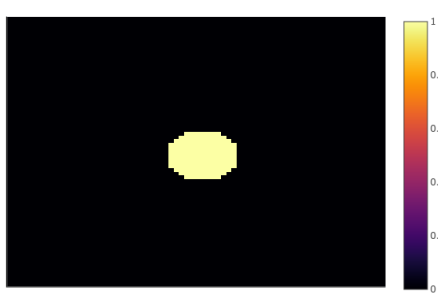


Figure 4.27: Single ultrasonic transducer element to be modeled

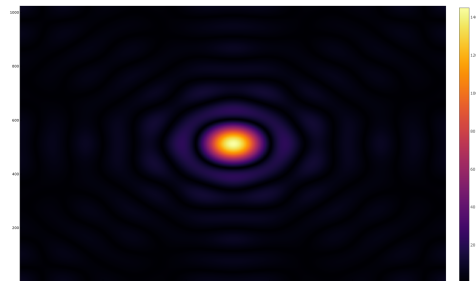


Figure 4.28: Approximate beam shape of a single ultrasonic transducer (Bore-sight view)

When viewed in three-dimensions, a single element produces the beam shape shown in figure 4.29.

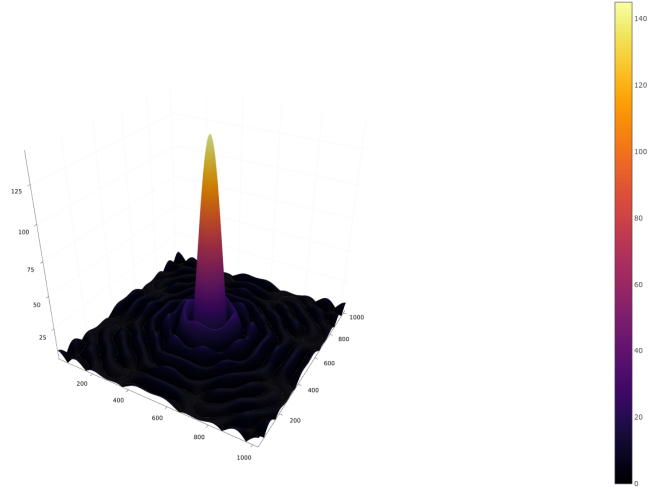


Figure 4.29: Approximate beam shape of a single ultrasonic transducer (3D view)

Extrapolating the single element into both the hexagonal and square packed designs was done by estimating the spacing between transducers according to a function that describes each designs layout and placing the transducer elements according to this spacing.

Square packed array simulation: The square pattern is shown below in figure 4.30 along with its bore-sight beam shape in figure 4.31.

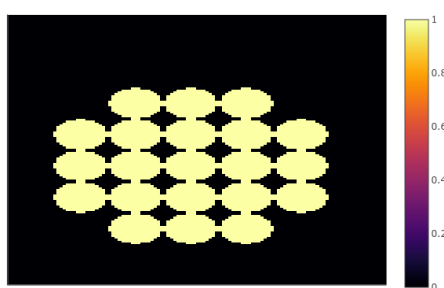


Figure 4.30: Square packed ultrasonic transducer elements to be modeled

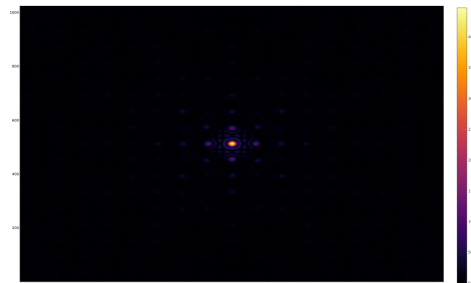


Figure 4.31: Approximate beam shape of the square packed ultrasonic transducer array (Bore-sight view)

The simulation shows that when many evenly spaced transducers are used, it produces a less smooth beam shape due to the discontinuities between elements. For the square packed circular array the beam shape appears to have a significant center lobe with moderately larger side lobes in comparison to the single element simulated in figure 4.29. Since this design has 21 elements, it would produce a larger sound pressure level at its peak than arrays with fewer elements, this factor should be taken into consideration when deciding on the design.

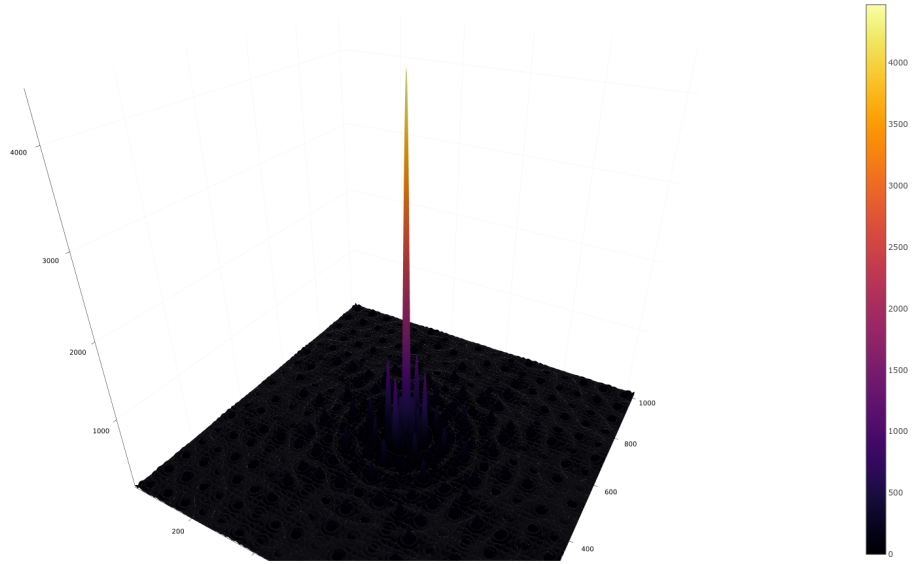


Figure 4.32: Approximate beam shape of square packed ultrasonic transducer array (3D view)

Hexagonally packed array simulation: The next simulation aims to reduce the spacing between transducer elements by use of hexagonal packing as shown in figure 4.19. This design has a filled fraction of 72.34% which should yield a more uniform beam shape since the discontinuities between transducers have been reduced from the square packed design with a filled fraction of 66.37% in figure 4.25. The magnitude of sound pressure energy in this design will be lower than the square design as it only has 19 elements instead of the 21 elements the square packed design contains.

The beam shapes were simulated for the hexagonally packed design and are presented in figures 4.33 to 4.36.

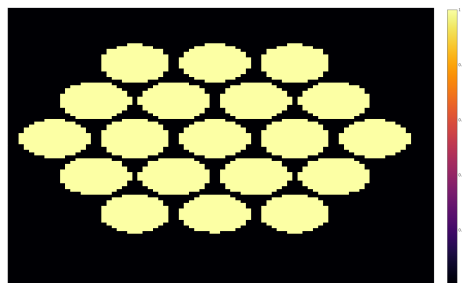


Figure 4.33: Hexagonally packed ultrasonic transducer elements to be modeled

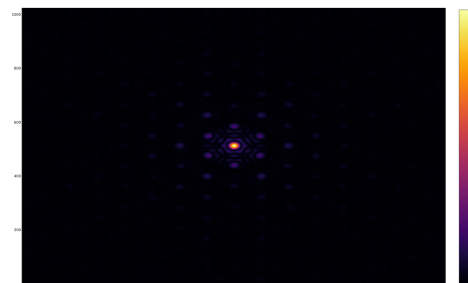


Figure 4.34: Approximate beam shape of the hexagonally packed ultrasonic transducer array (Bore-sight view)

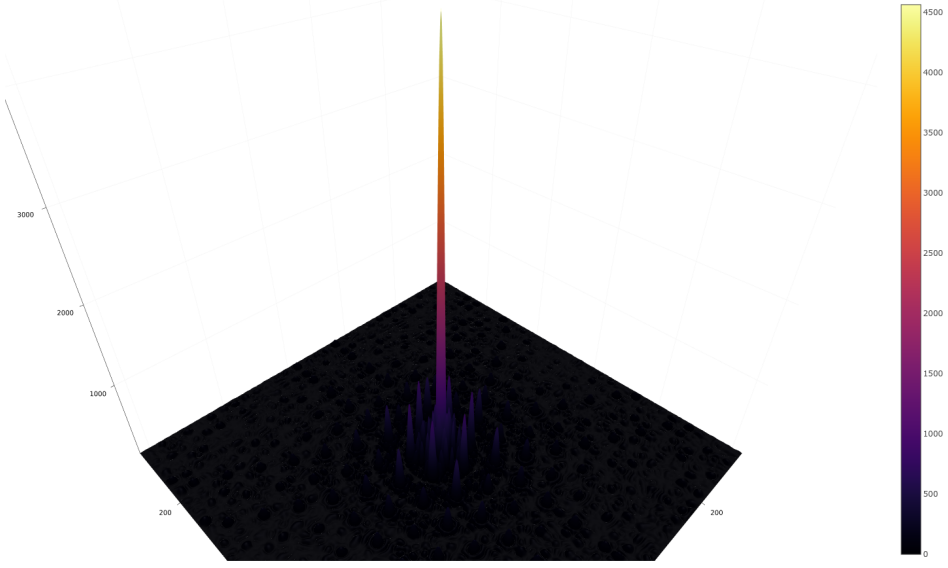


Figure 4.35: Approximate beam shape of hexagonally packed ultrasonic transducer array (3D view) with scale

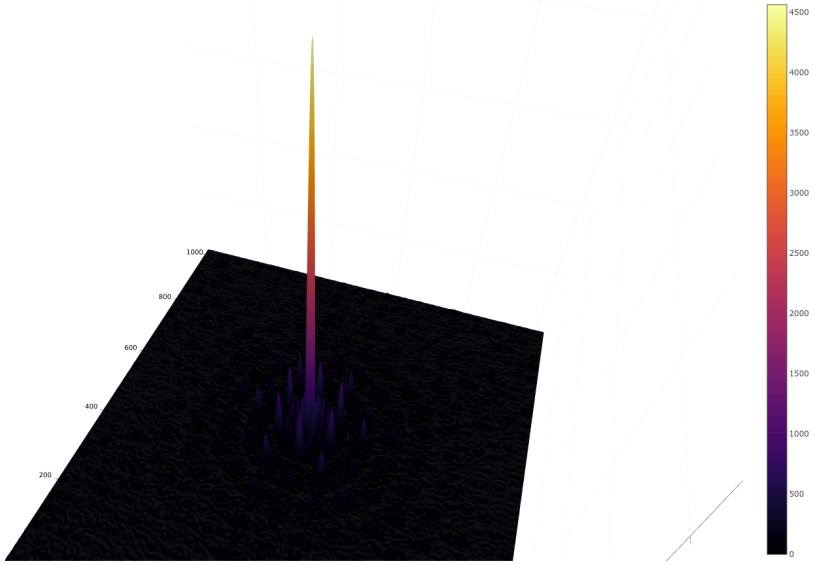


Figure 4.36: Approximate beam shape of hexagonally packed ultrasonic transducer array (3D shifted view to display sidelobes)

It can be seen that six side lobes appear when using the hexagonal design. This increased count of side lobes over the four side lobes present in the square packed array is undesirable; however; it does better approximate a single transducer's beam shape with the relatively small lobes surrounding the large main lobe thus representing a more uniform beam shape. Both the square and hexagonal beam results indicate a similar peak relative magnitude of the main

lobe of 4500, however; when analysing their bore-sight views the hexagonally packed array has six side lobes at approximate relative magnitude of 1000 while the square packed array has four side lobes with a relative magnitude of 1500. Neither result is fundamentally better than the other, but creating a beam with less side lobes would result in a more directive audio experience. Thus, since both results achieve a strong main lobe, the square packed solution is chosen going forward with the design as few side lobes is a more desirable trait for the directional audio system.

4.5.3 Array PCB design

Prior to the array design simulations done in the previous section, some alternative array designs were considered in the interest of creating a modular PCB design for better scalability. The rationale behind taking a modular approach is to reduce the risk of failure due to faulty transducers. With a monolithic design, failure of a few transducers could risk damaging surrounding transducers while adding difficulty in troubleshooting where the failed components are. The transducers chosen for this design are the Kibitone 400ST ultrasonic transducers. A custom footprint for this transducer was created using the dimensions in its datasheet and used for the PCB design in KiCAD.

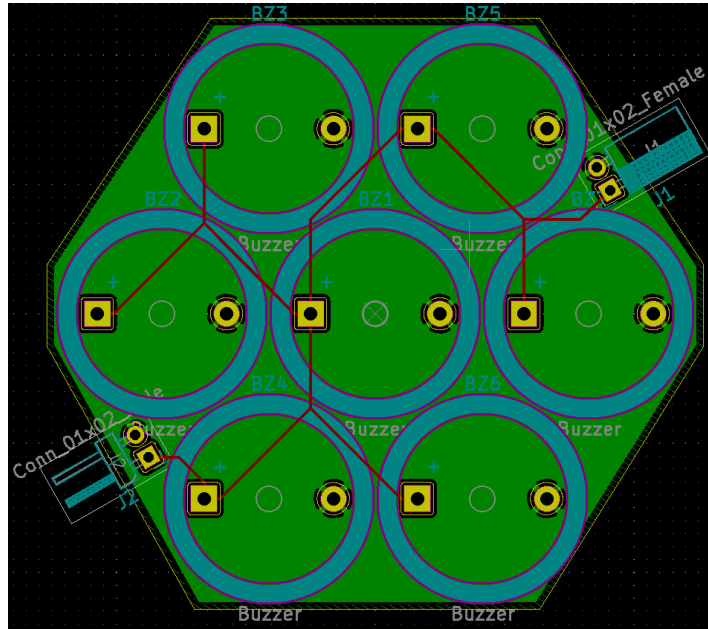


Figure 4.37: Rev 1.0 illustrating a modular octagonal design

Figure 4.37 demonstrates the first attempt at making a modular transducer array element. The idea behind this being that many octagons/hexagons can stack closely together providing minimal gaps between each PCB module. Rev 1.0 was used to estimate how best to layout the transducer and in what shape. This resulted in a octagonal design which only allowed 2 PCBs to interconnect as additional pin headers would be needed for a third module to link with the other two. Revision 1.1 is shown in figure 4.38 where additional pin headers were added to allow up to three hexagonal PCB modules to connect to each other as demonstrated by figure 4.39. Upon further development it was discovered that the male and female header pin placement was critical as exact alignment of them would be crucial for the modules to interconnect correctly with minimal gap. Adding to that, the centre of the array does not contain any transducers which would severely effect the uniformity of the beam. These factors drove the choice to redesign the array using a monolithic approach instead of modular and manage the risk faulty components create by additional component level testing during the implementation stage.

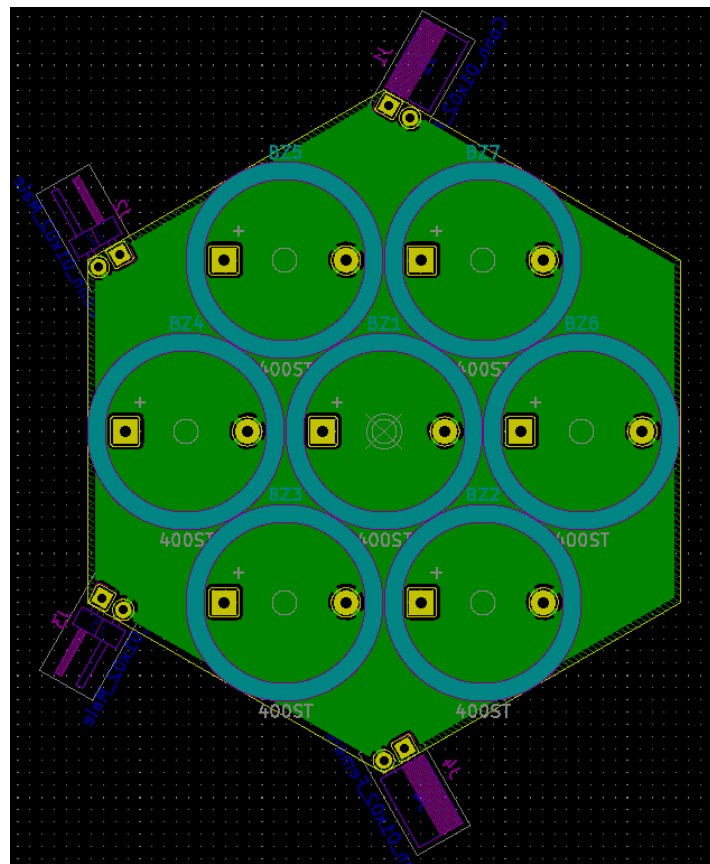


Figure 4.38: Rev 1.1 illustrating a modular hexagonal design with extra pin headers

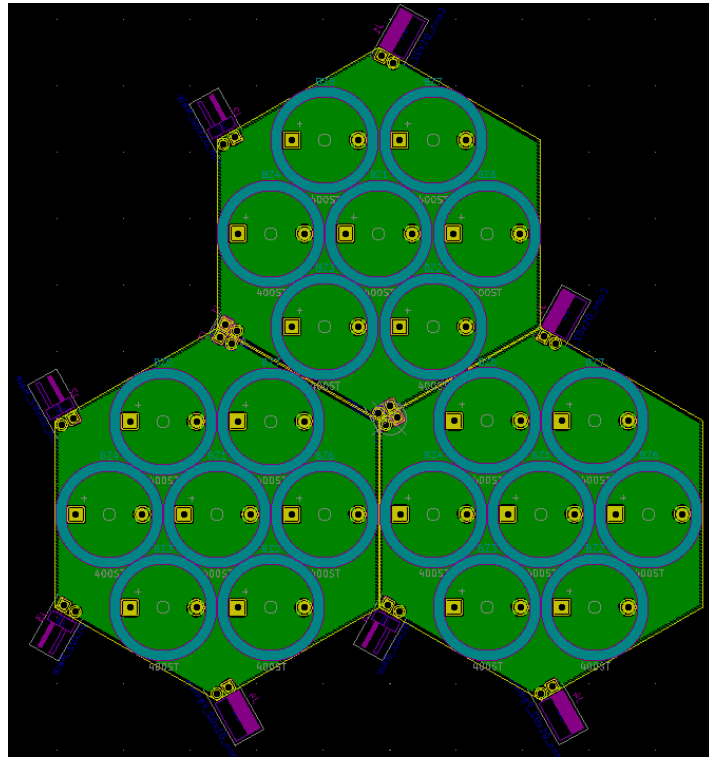


Figure 4.39: Three Rev 1.1 modular hexagonal PCBs interconnecting

Learning from the packing and beam shape simulations done in the previous sections, a circular PCB with square packing was chosen for the PCB implementation. Figure 4.40 illustrates the PCB design in KiCAD's PCB view while figures 4.41 and 4.42 show the 3D view of the circular PCB featuring a radius of 4.5cm. Note the 3D views use plastic piezoelectric buzzers as their 3D model, this is due to the adaption and reuse of an existing buzzer when creating the custom PCB footprint for the Kibitone 400ST ultrasonic transducer. This PCB features four mounting holes for M4 screws simplifying the arrays ability to attach to a testing setup. Additionally two sets of pin headers are provided allowing the signal to be fed in while being measured on the other set of pin headers.

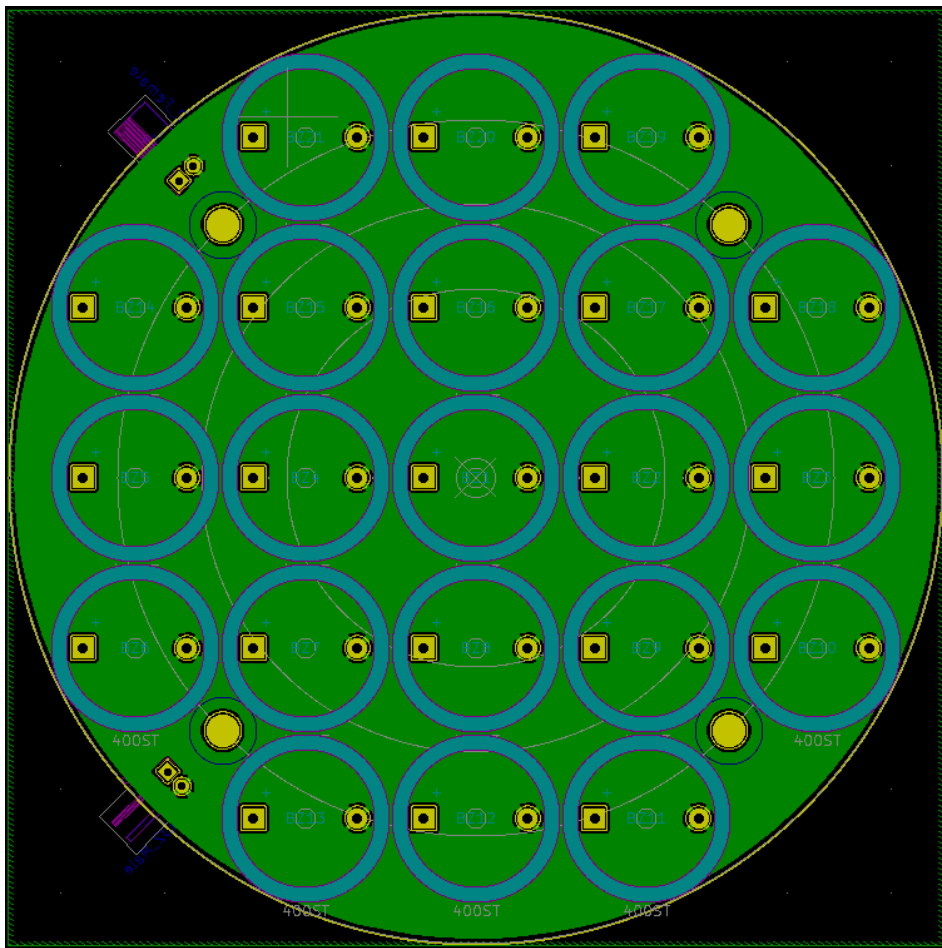


Figure 4.40: Rev 1.2 monolithic design derived from packing simulations

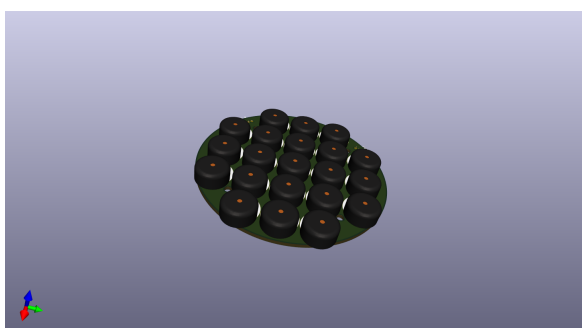


Figure 4.41: Isometric 3D view of Rev 1.2 Circular PCB design with square packing

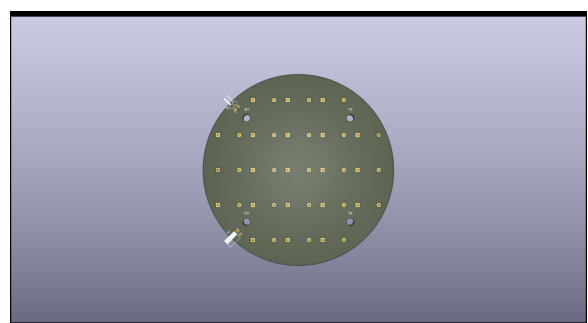


Figure 4.42: bottom 3D view of Rev 1.2 Circular PCB design with square packing

5 Implementation

The implementation section describes the process of constructing the directional audio system from the designs. This involves describing any deviations from the designs during implementation to achieve the desired goal of each subsystem.

5.1 Circuit construction

The circuits required for the directional audio system involve the construction of an analogue linear amplitude modulator using the AD633 as well the development of the power amplifier with the LM380 power amplifier.

5.1.1 AD633 Linear amplitude modulator implementation

The AD633 amplitude modulator was implemented as the designs intended on a breadboard. The circuit was powered by a ISO-Tech IPS 2303 2 channel DC power supply and supplied with the carrier wave by the Voltcraft FG1617 Function Generator. The implemented circuit is shown in figure 5.1 where the implemented circuit matches the design shown in figure 4.4.

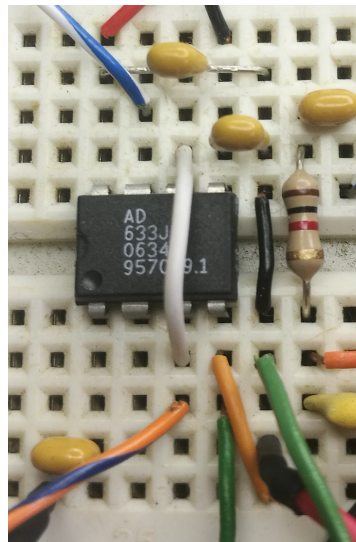


Figure 5.1: AM mixer implemented on breadboard

A test tone of 2.5 kHz is generated and input as the modulating waveform with a 40 kHz carrier input to the AD633 AM modulator and the outputs are shown in figure 5.2 and 5.3.

Figure 5.4 demonstrates the input modulating signal compared to the output AM signal. The output shows an approximate peak amplitude of 1.5V with a near zero amplitude for the negative half cycle. While this does not match up well with the expected output levels of the simulations; it is still an acceptable result for the subsystem. From these measurements the modulation index appears to lie around 50% using equation 9 given a carrier amplitude of 1V.

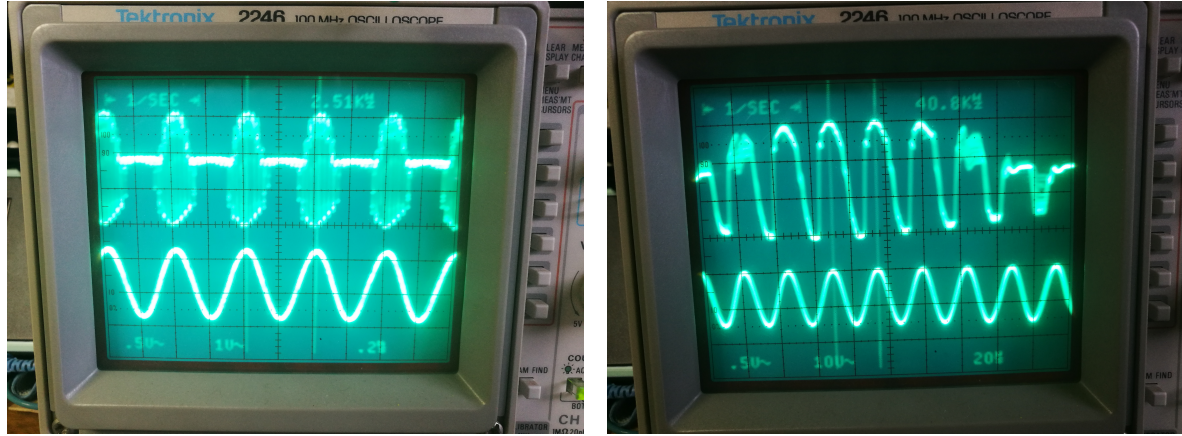


Figure 5.2: Input 2.5 kHz frequency compared to modulated output

Figure 5.3: Input 40 kHz frequency compared to modulated output

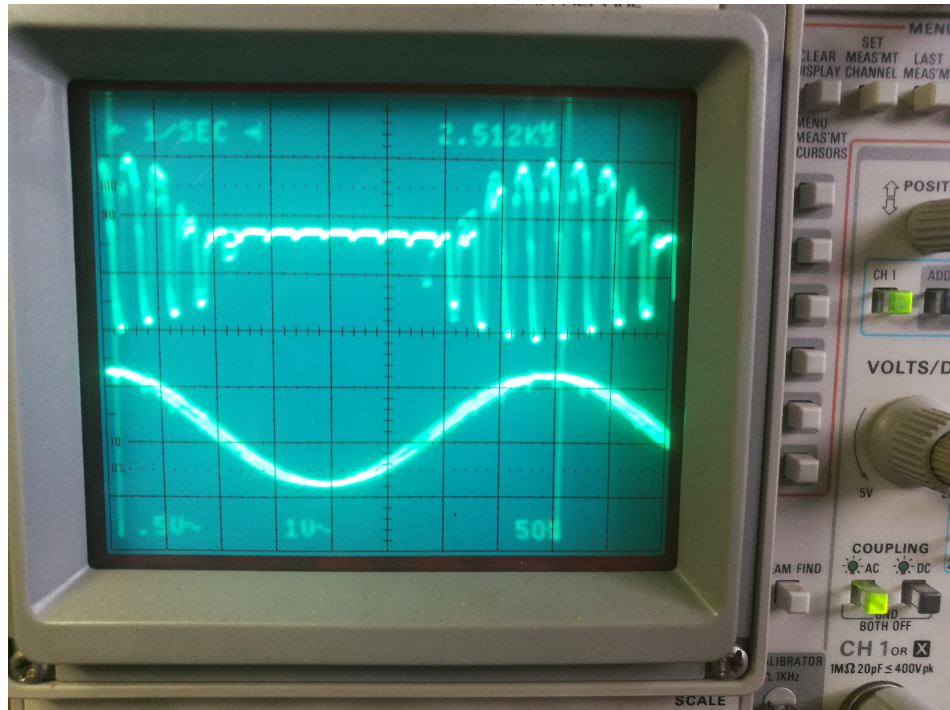


Figure 5.4: AM mixer output versus input signal

5.1.2 Amplifier Implementation

The implementation of the amplifier involved many small tweaks from the original design due to a low frequency oscillations occurring on the output. As such the final implementation involves many more components that were used to reduce these low frequency oscillations during the troubleshooting process. Figure 5.5 demonstrates the end result from the troubleshooting where the oscillations were under control. Figure 5.6 illustrates the new circuit after troubleshooting the low frequency oscillations.

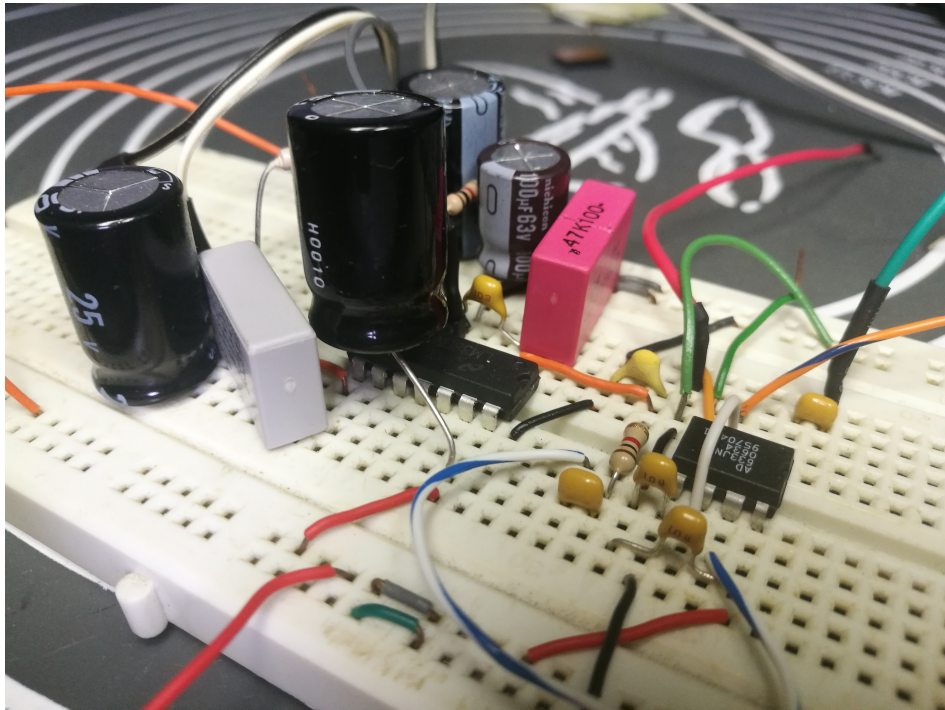


Figure 5.5: LM380 Power amplifier breadboard circuit after troubleshooting

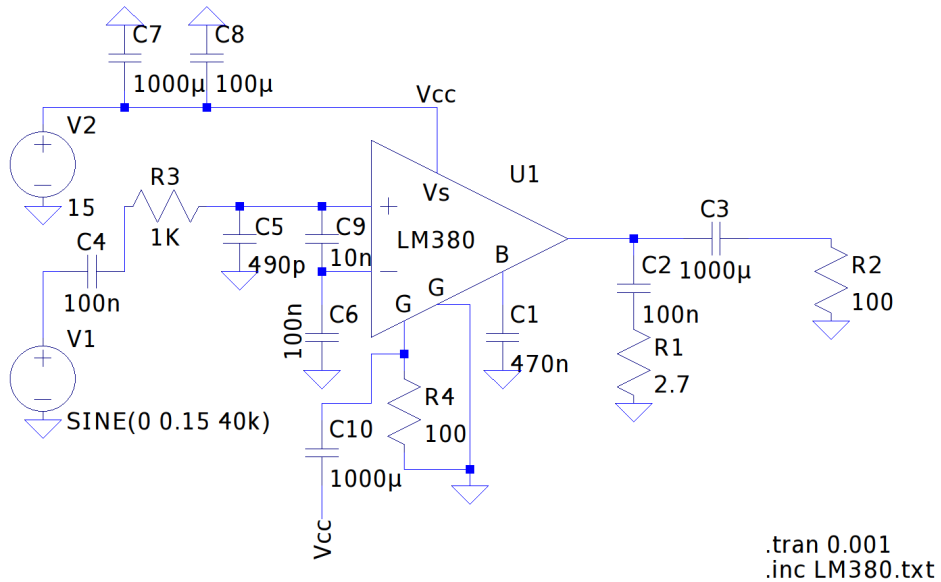


Figure 5.6: LM380 Power amplifier circuit schematic after troubleshooting

Upon application of a low frequency test tone of 500 Hz to a ordinary speaker, the amplifier produced an audible output with no low frequency oscillations. The output shown in figure 5.7 demonstrates the resultant output of the amplifier. The output only shows the positive half cycle of the wave due to the electrolytic capacitor present on the output, blocking the negative

half cycle. Unfortunately no alternative capacitors were readily available to correct this since the restrictions imposed by Covid-19 blocked access to components. Since the capacitor's main purpose is to smooth out the peaks for the $8\ \Omega$ speaker during this test, it can be bypassed when connecting the ultrasonic array.

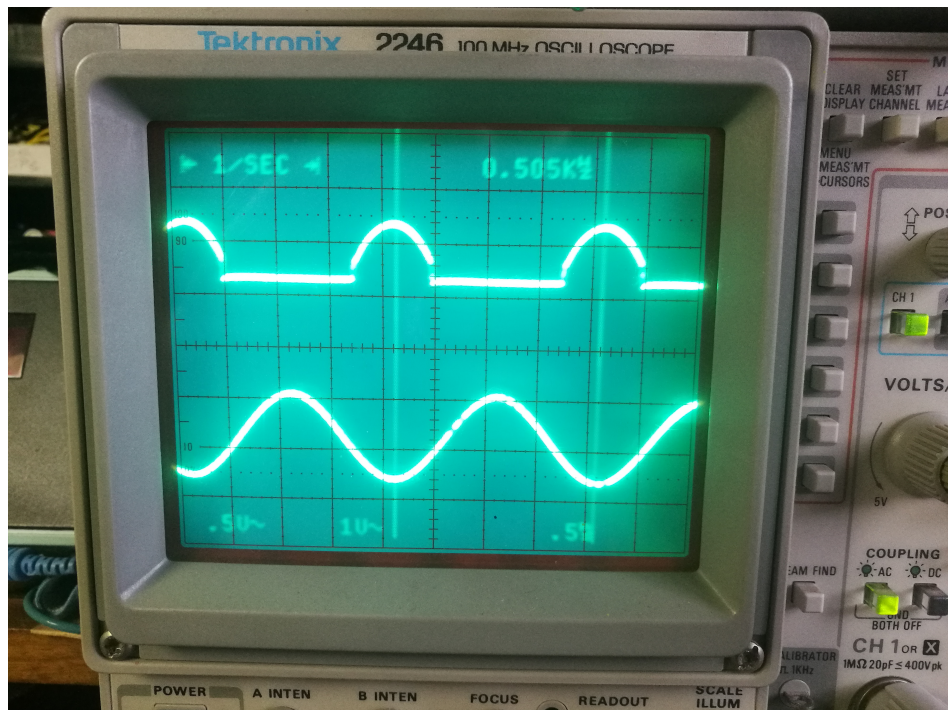


Figure 5.7: LM380 Power amplifier 500 Hz output to test speaker

5.2 Transducer array construction

The construction of the transducer array began once the previously designed PCBs arrived from JLC PCB. 21 Kibitone 400ST ultrasonic transducers were placed into the spaces provided by the PCB paying careful attention to the transducer orientation and soldered in place. Figures 5.8 and 5.9 show the unpopulated PCB and figures 5.10 and 5.11 show the PCB populated with the ultrasonic transducers. Additionally; M4 bolts with foam spacers, metal washers and nuts can be seen in the back view which are used for mounting in the tripod during testing.



Figure 5.8: Front side of unpopulated PCB

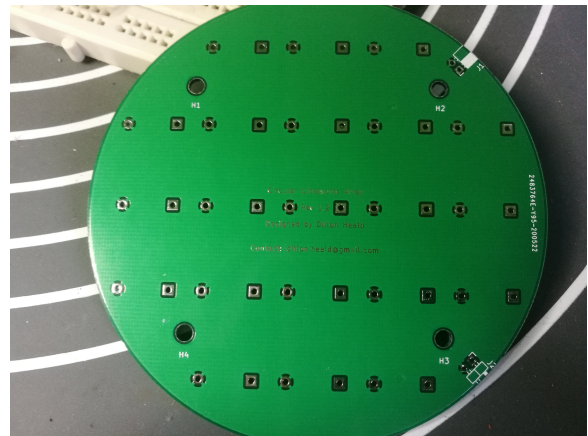


Figure 5.9: Back side of unpopulated PCB



Figure 5.10: Front side of populated PCB

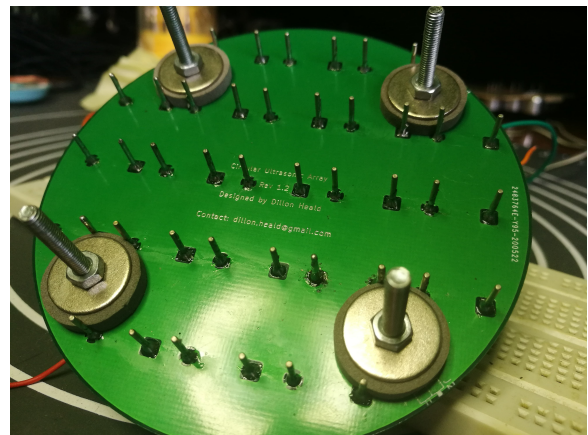


Figure 5.11: Back side of populated PCB

Once the PCB was populated, a 40 kHz tone was generated by the function generator and attached to the input of the PCB. Using 2 channels on a Tektronix 2246 oscilloscope, a receiver transducer was attached to one probe while the other probe was attached to the PCB's input signal allowing the output ultrasonic waves to be analysed and tested for any faults. The receiver transducer was passed over each emitting transducer and compared to the input signal, this test resulted in two transducers (BZ7 and BZ17 on the PCB) producing a 180°

phase shifted output as shown in figure 5.13 where the top trace is the received signal and the bottom trace is the input signal.

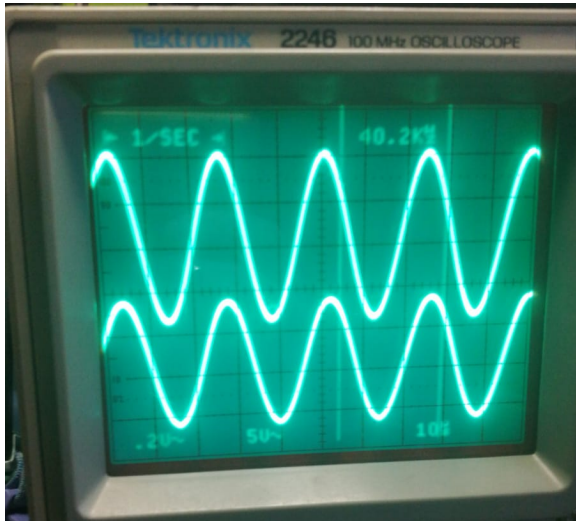


Figure 5.12: Transducer emitting in-phase output

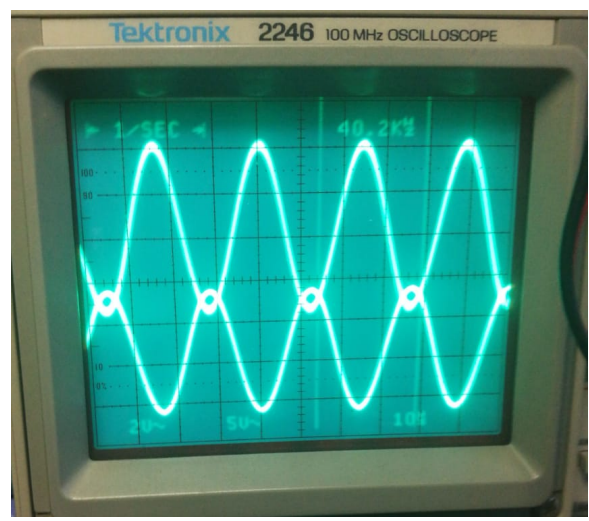


Figure 5.13: Transducer emitting out of phase output

To correct this phase inversion, ultrasonic transducers 7 and 14 were removed from the PCB and replaced with known working transducers. Each element in the array was once again tested and all transducers emitted an in phase output.

5.3 Pre-processing development

During signal simulation, Julia code was used to create and process the signals involved in the directional audio system. Naturally, it would be ideal if the output of this Julia code could be written to an audio port. Through some research, a library known as PortAudio was discovered which claimed to have exactly this ability, however; it is designed for C, C++ and requires a wrapper to work with Julia. The wrapper [15] allows for sampled signals to be written to the audio interface as long as they are values between ± 1 . Adapting the code shown in the simulation section to record audio, process and play the processed output through the computers audio interface required a few adaption such as high pass filtering and signal level shifts and is shown in full in appendix A under listing 8. The result of this implementation produced a reduced in magnitude output due to the repeated integration which was corrected for by increasing the output amplitude by a tuned factor. Upon input into the modulator, passing through the amplifier and into the ultrasonic transducer array, the signal was heavily distorted. To troubleshoot this, the integration of the signal was removed and the signal was instead only shifted above zero and square-rooted. This resulted in a far less distorted output by the transducer array. Since the output was now more intelligible, a new Julia program was developed that only performed the signal shift and square-root operation on a generated tone of 2.5 kHz. This pre-processed tone could be adjusted in length up to 60 seconds as PortAudio has a limitation on the size of its output buffer. This code is used to generate the pre-processed audio for use in the beam sweep tests further elaborated on in the testing methodology section. Figures 5.14 and 5.15 demonstrate the inputs and outputs of the pre-processing Julia program using only square-root, filtering and level shifting processing.

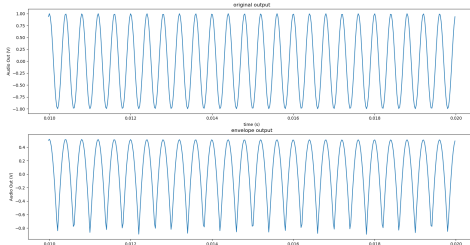


Figure 5.14: Time domain representation of original tone and output pre-processed tone

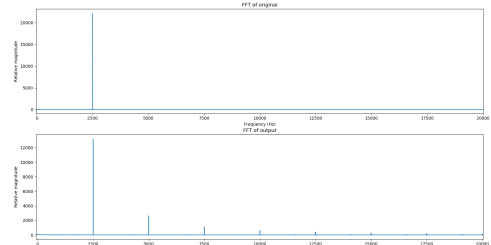


Figure 5.15: Frequency domain representation of original tone and output pre-processed tone

6 Testing Methodology

The testing and verification of the directional audio system will be done by comparing its acoustic performance with a traditional loudspeaker. Particular test points of interest include the directionality of the speaker and the audible harmonic distortion for pure tone cases.

6.1 Test setup and apparatus

The test setup for recording results from both the traditional and ultrasonic directional speaker involves the items shown in table I.

| Item name | Function |
|---------------------|-----------------------------------------------------------------------------------------------------------------------------------|
| Tripod | Stable platform to pan the speaker through a consistent arc |
| Microphone | Rhode NT1 Cardioid condenser microphone provides a flat frequency response with a front facing cardioidal recording beam pattern. |
| ADC | Focusrite Scarlett 8i6 audio interface provides a 24 bit recording at 44.1 kHz sample rate. |
| Recording software | Abelton Live version 10.1.15 used to capture and edit the recording. |
| Laptop/Julia | A laptop running Julia version 1.3.1 produces the processed and unprocessed audio. |
| Signal generator | Produces the 40 kHz carrier wave |
| Mixer | Mixes the baseband audio with the 40kHz carrier to produce AM signal for ultrasonic speaker. |
| Power amplifier | Amplifies the signal to $\pm 26V_{p-p}$ and supplies sufficient power to drive the ultrasonic transducer array. |
| Ultrasonic array | This is the constructed ultrasonic array which will emit the directional audio beam. |
| Traditional speaker | A regular loudspeaker taking in only baseband audio from the laptop. |

Table I: Table of apparatus used during testing

These items were placed in a room with 1.75m separating the centre of the ultrasonic / traditional speaker from the microphone. Figure 6.1 shows the top down representation of the test setup in a square room. Ideally the test should be done in a larger room with less reflective surfaces; however, due to the Covid-19 pandemic testing resources were limited to what was available at home.

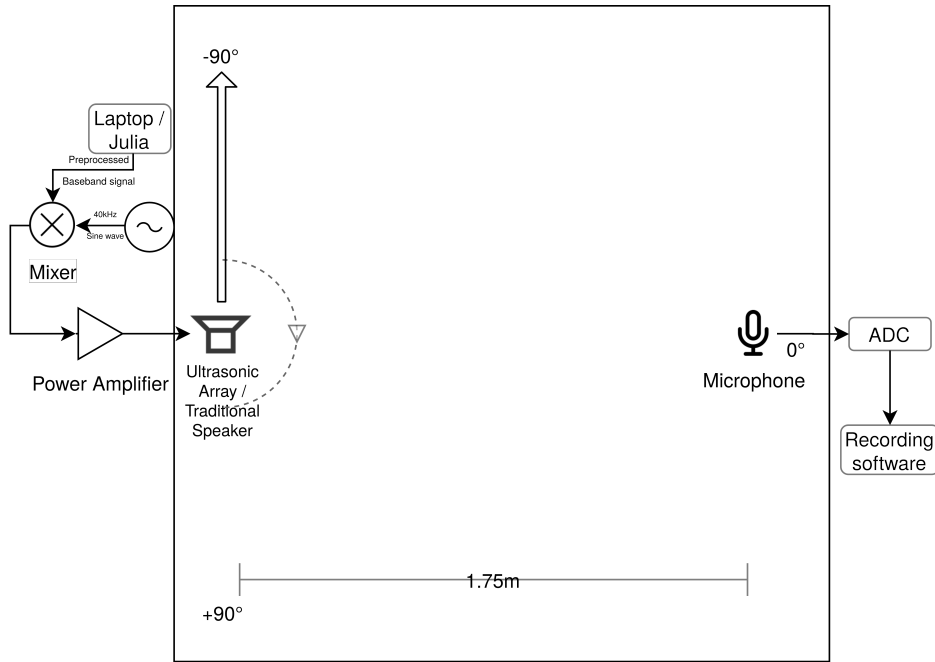


Figure 6.1: The test setup used for distortion and directionality testing.

6.2 Distortion testing method

To test distortion, the ultrasonic array is directed 0° relative to the microphone (head on) and both a pre-processed and unprocessed 2.5 kHz sine wave are generated in Julia, modulated by the mixer and emitted with the array in two separate recordings. One recording for only pre-processed audio and one for no processing and only amplitude modulation.

The ultrasonic array is then removed from the tripod and replaced with a traditional speaker. With the speaker facing the same direction as before and using Julia on the laptop, a 2.5 kHz sine wave is generated and played by the speaker without any modulation or processing done on the waveform. Each recording is captured for 15 seconds and edited to only include the period where the signal is audible and no other sources of noise are visible in the waveform. These recordings are then imported into Julia and analysed. For each recording, the FFT of the recording is produced to analyse the fundamental frequency magnitude relative to its harmonics. This provides a measure to determine how distorted the output of the speaker is by comparing how close the magnitude of the harmonics is to the fundamental frequency.

6.3 Directionality testing method

To test directionality, the ultrasonic array is initially directed to -90° relative to the microphone and the pre-processed 2.5kHz sine wave is generated using Julia, modulated with the mixer and emitted from the array. A operator then positions themselves behind the tripod and slowly pans the speaker from -90° through 0° and finally ending at $+90^\circ$. The recording is then stopped and edited to only include the period over which the array is swept to reduce operator noise affecting the results.

A similar method is followed for the traditional speaker directionality test. Beginning at -90° , a 2.5kHz sine wave is created in Julia and played by the speaker. The same beam sweep method occurs as in the ultrasonic array case and the recording is stopped at the end of the sweep.

The recordings are edited to only include the period of the beam sweeping and thus, should produce a maximum near the middle of the recorded time. The FFT for the whole spectrum of the samples is then generated along with the time domain representation of the recorded signal to provide context to what is actually heard during the beam sweep by the microphone. The recordings are then filtered by use of a band-pass FIR filter in the frequency domain using Julia with a bandwidth of 100 Hz. The band-pass filter is then centred on the fundamental frequency (2.5 kHz), the first harmonic (5 kHz) and the second harmonic (7.5 kHz) and the time domain representations of the filtered outputs are plotted.

The filtering provides a higher signal to noise ratio for the testing signals, thus providing a clearer representation in the time domain of each of these frequencies and how intense they are over the period of the sweep. The time domain representations should indicate how intense each of these frequencies are, especially as they approach the 0° angle in the sweep and will produce an approximate beam shape for the directional audio system and the traditional speaker to compare it to.

In ideal circumstances, this test could be done with an accurate angle of incidence by using a motor driven platform and recording the signal at set increments in angle. That data could then be used to construct a more accurate beam pattern. This however, was not possible due to restricted access to lab resources as this testing is done during the Covid-19 pandemic. As a result, only an approximate beam shape can be resolved since the angle of incidence is unknown.

7 Results

To test the distortion and directionality of the directional speaker, recordings were made where a 2.5 kHz tone was generated, appropriately pre-processed using Julia and produced into the testing environment by the ultrasonic directional speaker. The distortion was compared to a classical loudspeaker and the same ultrasonic directional speaker but without the pre-processing provided by the Julia code. The directivity testing was achieved by sweeping the transducer array and classical loudspeaker across the microphone at a distance of 1.75m. The arc transitioned the speaker faces between -90° to $+90^\circ$ relative to the microphone. Following these tests, the recordings were imported into Julia where they were processed with appropriate filtering and transformation to demonstrate the directionality and distortion of the ultrasonic directional speaker.

7.1 Distortion testing

The distortion testing of the square root AM system is expected to produce a fundamental signal at 2.5kHz with decreasing magnitudes for 1st and 2nd harmonics at 5kHz and 7.5kHz respectively. The same tests without the square root pre-processing applied should produce larger magnitude harmonics while the traditional loudspeaker should produce little to no harmonics.

7.1.1 Traditional loudspeaker distortion results

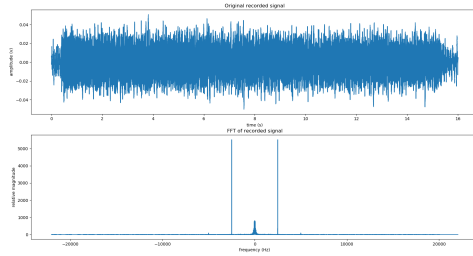


Figure 7.1: The spectrum and time domain signal of the traditional loudspeaker with a 2.5kHz input tone

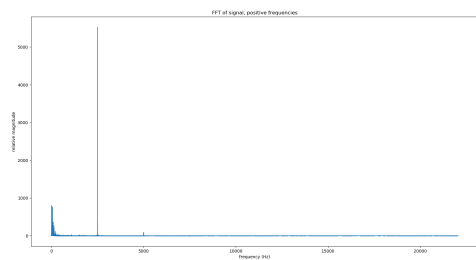


Figure 7.2: The positive spectrum of the traditional loudspeaker with a 2.5kHz input tone

The results in figure 7.1 and 7.2 indicate a strong presence of the 2.5kHz test tone with some smaller low frequency noise likely caused by background noise as well as a small 1st harmonic at 5kHz.

7.1.2 Square-root AM versus AM ultrasonic directional speaker distortion results

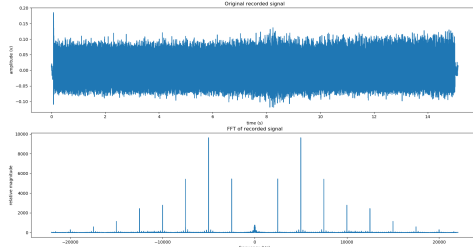


Figure 7.3: The spectrum and time domain signal of the square root amplitude modulated ultrasonic speaker with a 2.5kHz input tone

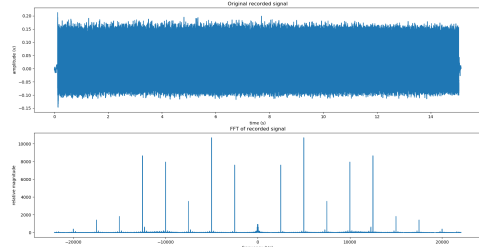


Figure 7.5: The spectrum and time domain signal of the amplitude modulated ultrasonic speaker with a 2.5kHz input tone

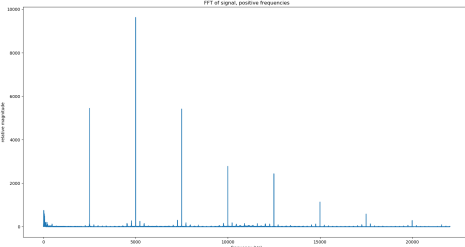


Figure 7.4: The positive spectrum of the square root amplitude modulated ultrasonic speaker with a 2.5kHz input tone

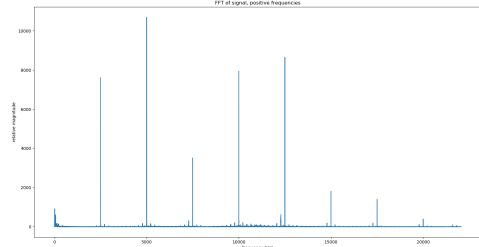


Figure 7.6: The positive spectrum of the amplitude modulated ultrasonic speaker with a 2.5kHz input tone

The results in figure 7.3 and 7.4 for the ultrasonic directional speaker with square root pre-processing show a strong tone at the 1st harmonic of the test tone (5kHz). This result appeared only when the microphone was placed into the ultrasonic beam as figures 7.7 and 7.8 show the results for the ultrasonic beam being directed away from the microphone. The signal levels are lower than the original result but the fundamental frequency now lies on 2.5kHz.

The results of the ultrasonic directional speaker without any pre-processing are presented in figures 7.5 and 7.6. Comparing the spectrum of the speaker to the square root AM system in figures 7.3 and 7.4, the harmonics appear to be even more pronounced and amplified when no pre-processing is applied. Figure 7.6 indicates the 1st harmonic to be the largest, followed by the 4th harmonic, then 3rd and finally the fundamental. Additionally, the magnitudes of these harmonics are larger than the square root AM tests.

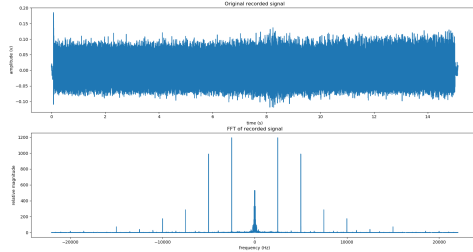


Figure 7.7: The spectrum and time domain signal of the square root amplitude modulated ultrasonic speaker (microphone outside of beam) with a 2.5kHz input tone

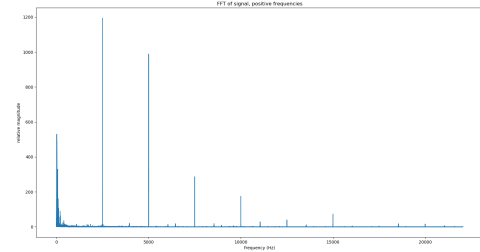


Figure 7.8: The positive spectrum of the square root amplitude modulated ultrasonic speaker (microphone outside of beam) with a 2.5kHz input tone

7.2 Directivity testing

The test setup for directivity testing involved sweeping the transducer/speaker in an arc such that the center of the radiated beam sweeps from left to right of the microphone while producing a tone. The recordings were then cut to the length of the sweep and filtered to demonstrate the signal level of the fundamental 2.5kHz tone as well as its 1st and 2nd harmonics at 5 and 7.5 kHz respectively.

7.2.1 Directivity of a traditional loudspeaker

The unfiltered recording of the loudspeaker beam sweep is analysed in figure 7.9 where the time and frequency domain representations of the signal are presented for the loudspeaker beam sweep.

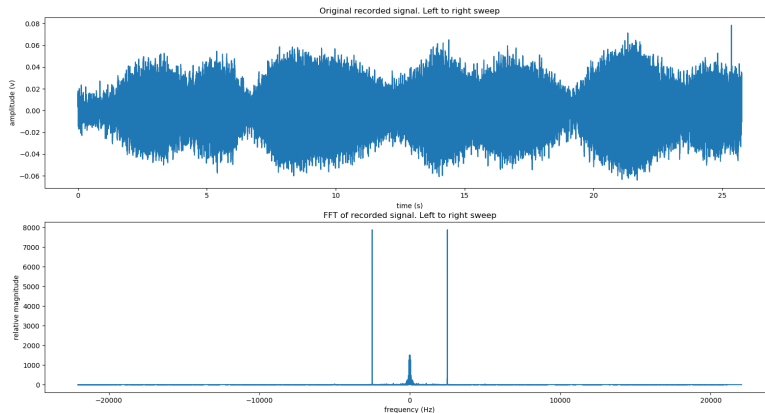


Figure 7.9: Original beam sweep recording and FFT of all samples for traditional loudspeaker

Filtered 2.5 kHz beam sweep results Figures 7.10 and 7.11 show the time and frequency domain representations of the recorded beam sweep for a traditional loud speaker. Figure 7.10 demonstrates a mostly consistent volume for the duration of the entire beam sweep, oscillating between approximately ± 0.04 V with the smallest troughs at around 7 and 19 seconds. The maximum peaks occur at approximately 9 and 22 seconds which are just after the aforementioned troughs. The results represent a signal without significant directionality as similar sound pressure levels and thus, recorded amplitudes are measured throughout the beam sweep. The spectrogram in figure 7.11 demonstrates what portion of the spectrum was used to create the time domain signal in figure 7.10 but does not show significant variation in signal magnitude over the sweep.

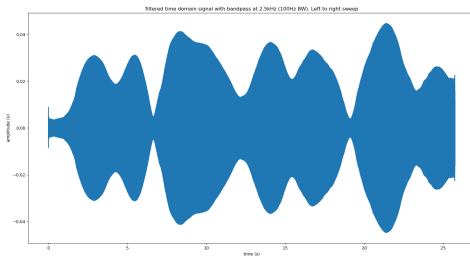


Figure 7.10: Filtered 2.5kHz time domain signal emitted from a traditional speaker over beam sweep

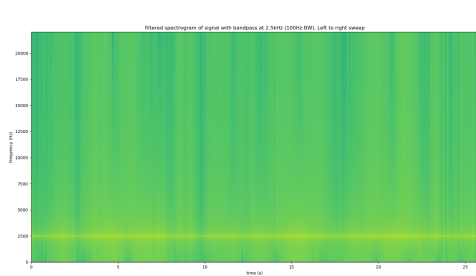


Figure 7.11: Filtered 2.5kHz spectrum emitted from a traditional speaker over beam sweep

5 kHz beam sweep results Figures 7.12 and 7.13 show the time and frequency domain representations of the recorded beam sweep for a traditional loud speaker band-pass filtered at 5kHz. Figure 7.12 demonstrates a lot more peaks and troughs over the entire beam sweep, oscillating between approximately ± 0.0004 V with the smallest troughs at around 9 and 20 seconds. The maximum peaks occur at approximately 14 and 22 seconds. The results represents a signal without significant directionality as there is not a significant peak near the middle of the data. The spectrogram in figure 7.13 demonstrates what portion of the spectrum was used to create the time domain signal in figure 7.12 but does not show significant variation in signal magnitude over the sweep, much like the 2.5kHz filtered result.

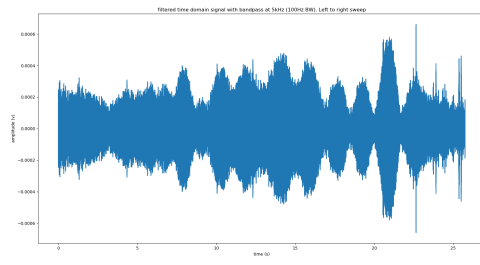


Figure 7.12: Filtered 5kHz time domain signal emitted from a traditional speaker over beam sweep

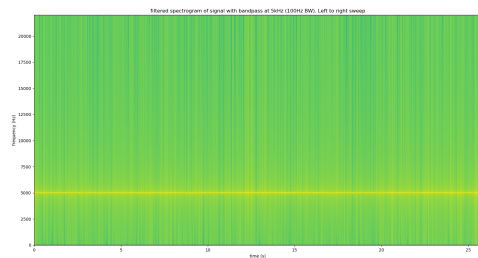


Figure 7.13: Filtered 5kHz spectrum emitted from a traditional speaker over beam sweep

7.5 kHz beam sweep results Figures 7.14 and 7.15 show the time and frequency domain representations of the recorded beam sweep for a traditional loud speaker band-pass filtered at 7.5kHz. Figure 7.14 demonstrates few peaks over the entire beam sweep at relatively low magnitudes. The maximum peak should occur between 10 to 15 seconds if this were a directional beam but they instead appear before and after this region. The spectrogram in figure 7.15 demonstrates what portion of the spectrum was used to create the time domain signal in figure 7.14 but does not show significant variation in signal magnitude over the sweep, much like the 2.5kHz filtered result.

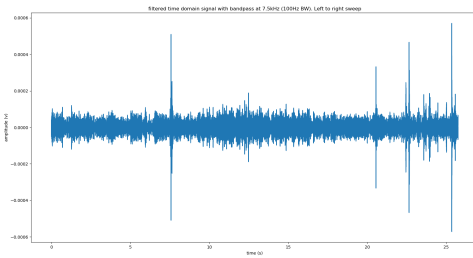


Figure 7.14: Filtered 7.5kHz time domain signal emitted from a traditional speaker over beam sweep

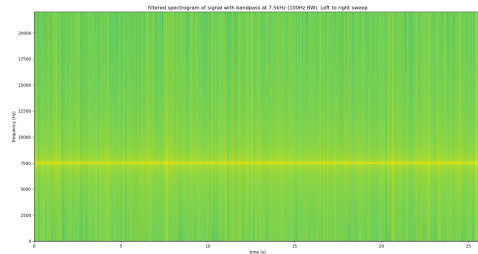


Figure 7.15: Filtered 7.5kHz spectrum emitted from a traditional speaker over beam sweep

7.2.2 Directivity of the directional audio system

The results for the directional audio speaker are expected to show a significant spike in signal near the middle (10-15 seconds) as this is when the ultrasonic speaker's directional beam is in line with the microphone. The unfiltered recording of the ultrasonic directional speaker beam sweep is analysed in figure 7.16 where the time and frequency domain representations of the signal are presented for the ultrasonic directional speaker beam sweep.

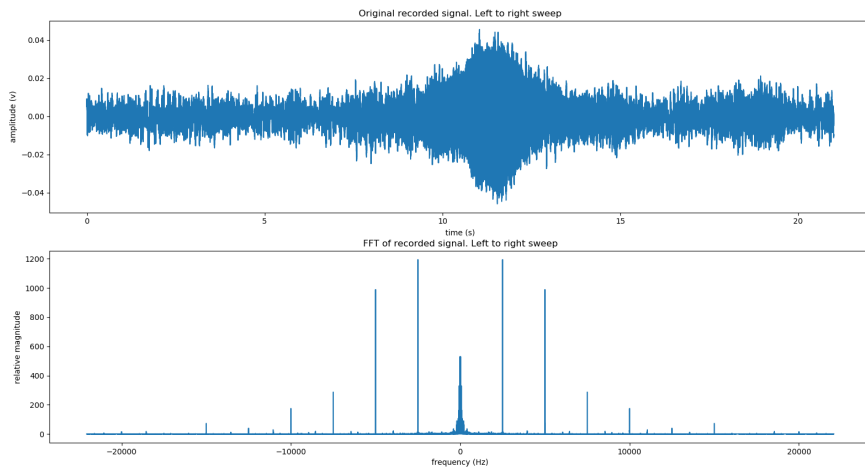


Figure 7.16: Original beam sweep recording and FFT of all samples for a ultrasonic directional speaker

Filtered 2.5 kHz beam sweep results Figures 7.17 and 7.18 show the time and frequency domain representations of the recorded beam sweep for a ultrasonic directional speaker filtered to show the 2.5kHz fundamental tone.

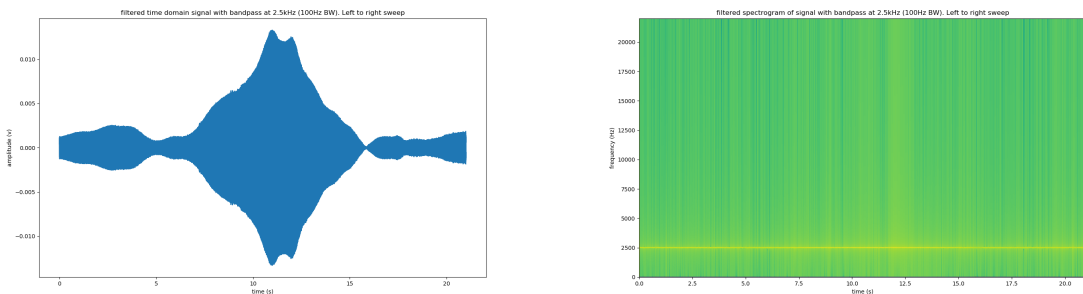


Figure 7.17: Filtered 2.5kHz time domain signal emitted from a ultrasonic directional speaker over beam sweep

Figure 7.18: Filtered 2.5kHz spectrum emitted from a ultrasonic directional speaker over beam sweep

Figure 7.17 shows a large spike in signal amplitude as the beam crosses the microphone with tapered edges on either side of this spike. Some minor fluctuations in the 2.5kHz signal are present before and after this spike and are likely from reflections of the beam off surfaces in the room. Note that there are two similarly sized maximum spikes at the apex of the sweep which may be the result of the beam reflecting off the wall behind the microphone, then passing over the microphone (causing the dip) and then reflecting once more. The spectrogram in figure 7.18 demonstrates what portion of the spectrum was used to create the time domain signal in figure 7.17 and shows some increase in intensity as the recording reaches the 11 second mark.

Filtered 5 kHz beam sweep results Figures 7.19 and 7.20 show the time and frequency domain representations of the recorded beam sweep for a ultrasonic directional speaker band-pass filtered to only show the 5kHz harmonic. Figure 7.19 shows a large spike in

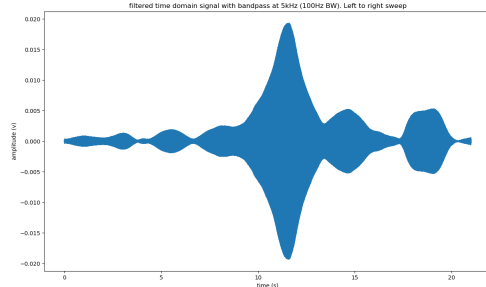


Figure 7.19: Filtered 5kHz time domain signal emitted from a ultrasonic directional speaker over beam sweep

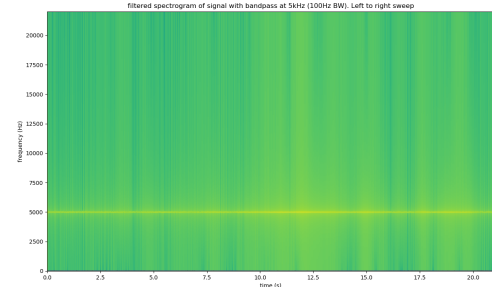


Figure 7.20: Filtered 5kHz spectrum emitted from a ultrasonic directional speaker over beam sweep

signal amplitude as the beam crosses the microphone with tapered edges on either side of this spike at 11 seconds. Before and after this main spike there exists some similarly shaped peaks in amplitude which could be the result of the side lobes of the beam as shown during the simulations in figure 4.31 and figure 4.32. Alternatively it could be the result of reflections within the room causing pockets of constructive interference. Note however this is the first harmonic of the fundamental tone (2.5kHz) being produced which makes it somewhat undesirable as it is not the original tone intended to be produced. The magnitude of the main lobe's spike reaches near 0.04 V peak to peak, which is larger than the fundamental in figure 7.17. The shape of the main lobe is a lot narrower for the 5kHz harmonic than the 2.5kHz tone indicating that the first harmonic is a more directional beam than the fundamental while having larger side lobes than the 2.5kHz fundamental tone. The spectrogram in figure 7.20 demonstrates what portion of the spectrum was used to create the time domain signal in figure 7.19 and shows more intensity near the 11 second mark.

Filtered 7.5 kHz beam sweep results Figures 7.21 and 7.22 show the time and frequency domain representations of the recorded beam sweep for a ultrasonic directional speaker band-pass filtered to only show the 7.5kHz harmonic. Figure 7.21 shows a large spike in

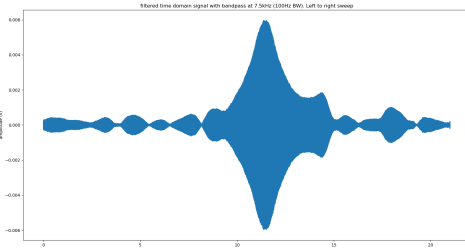


Figure 7.21: Filtered 7.5kHz time domain signal emitted from a ultrasonic directional speaker over beam sweep

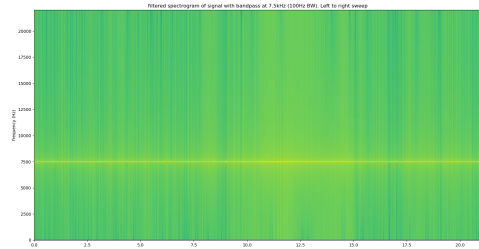


Figure 7.22: Filtered 7.5kHz spectrum emitted from a ultrasonic directional speaker over beam sweep

signal amplitude as the beam crosses the microphone with tapered edges on either side of this spike at 11 seconds. Before and after this main spike there exists some peaks in amplitude elsewhere in the beam sweep which are likely the result of reflections within the room causing pockets of constructive interference but could also indicate the presence of side lobes. Since this is the 2nd harmonic of the fundamental tone (2.5kHz) we would expect it to be of a significantly lower amplitude than the fundamental, which it does achieve with a peak to peak value of 0.012 V. This makes it still audible but at a lower intensity than the 1st harmonic and the fundamental (which are at similar intensities). The shape of the main lobe is a lot narrower than the 2.5kHz result and has a similar sharpness to the 5kHz harmonic indicating that both the first and second harmonic are more directional beams than the fundamental tone. An asymmetry occurs for the 7.5kHz harmonic as the beam leaves the microphone. The intensity appears to taper off at a similar rate to its initial rise to the peak but then begins increasing again. This could be due to an asymmetric beam pattern or simply the corner of the room reflecting the directional beam back to the microphone and causing constructive interference. The spectrogram in figure 7.22 demonstrates what portion of the spectrum was used to create the time domain signal in figure 7.21 and shows more intensity as the recording approaches the 11 second mark, followed by a reduction in intensity.

8 Discussion & Conclusion

This section discusses the results from the tests and the project as a whole. The results for the entire directional audio system are then summarised in the conclusion while providing suggestions for future avenues of work for the project.

8.1 Discussion

The results from the distortion and directivity tests provided real world data on the low cost implementation of a directional audio system. Due to the real world nature of these results, some noise is present which was minimised as best as possible.

Distortion result discussion: The distortion results for the traditional loudspeaker came out as expected. A large 2.5 kHz tone was present with relatively small magnitude low frequency noise. Unexpectedly, the traditional loudspeaker produced a very low magnitude 1st harmonic at 5 kHz. This 1st harmonic's presence could likely be an artefact in the Julia code used to produce this test tone as the output may have clipped what the audio jack is capable of. While the 1st harmonic's presence is visible in the spectrum of the recorded data, it is not discernible to human hearing and should not be considered a significant form of distortion due to its low relative magnitude compared to the 2.5 kHz fundamental and as such is a good control for the tests.

The ultrasonic directional speaker distortion results provided insight into what the pre-processing does to the magnitude of the harmonics. From Kite's results [5], one expects the square-root AM (SRAM) technique to result in lowered harmonic distortion compared to the pure AM case. The results show that the pure AM output without pre-processing has seemingly asymmetric distribution of harmonic magnitudes while the SRAM pre-processed results demonstrate a more natural and symmetrical distribution of harmonics. The high magnitude of the 1st harmonic is an unexpected result but is shown to perhaps be an issue with the interaction of the ultrasonic beam and the microphone since the 2.5 kHz tone is the strongest magnitude when the beam is slightly off centre from the microphone. Close inspection of these spectrums reveals small magnitude side tones of each of the major tones which appear to be similar to what was shown in the signal simulations for the square-rooted signal featuring a large exponential decay of these side tones. The higher frequency harmonics are undesirable as they create distortion, however; the distortion is reduced for the SRAM pre-processed result since its harmonics all appear to drop off at a near exponential rate. The presence of the large 5 kHz tone could have to do with the beam reflecting off of the wall behind the microphone since the off beam result shows a stronger presence of the 2.5 kHz tone. This 5 kHz presence could also be the result of an imperfect squaring by the environment due to the small distance between the transducers

and the microphone; resulting in a difference frequency slightly off the expected baseband frequency seen in simulations. One final factor that could be the issue is the use of large carrier amplitude modulation. Since the carrier is larger than the side lobes where the signal lies, the difference frequency that the environment creates during its demodulation could result in this carrier adding energy to a particular frequency in its side bands due to harmonics.

Directivity result discussion: The directivity results for the traditional loudspeaker showed a relatively consistent signal level through its sweep. There were some notable troughs in the filtered cases which are likely the result of the environment reflecting and absorbing varying amounts of sound pressure. For all the filtered cases, no main peak in signal level coincided with the beam crossing the centre of the microphone. This demonstrates the relatively low directivity of conventional loudspeakers and aside from some inconsistencies in signal level due to reflections in the testing environment, can be considered a good control representation of a non-directional loudspeaker.

The results for directionality testing of the directional audio system demonstrated the real world representation of what the system sounds like to human hearing relatively well. When the beam is experienced, a clear difference in sound is heard depending on which ear is in the beam. During testing only one microphone was used and the waveform it recorded represents what is heard quite well. Before the directional audio beam reaches the microphone, subtle magnitudes of the test tone can be heard in the environment as shown by the 2.5 kHz filtered result. As the beam approaches the microphone, a sudden increase in volume occurs, thus demonstrating significantly more directionality than the loudspeaker. A similar gradient in drop off of signal loudness is experienced as the microphone exits the beam until the signal level is returned to the level before the beam reached the microphone. Further filtering of the 1st and 2nd harmonic revealed that these tones are more directional than the original test tone of 2.5 kHz. Since the beam angle is directly proportional to wavelength, thus; inversely proportional to frequency as per equation 1, this result makes some sense as the beam angle is reduced as the frequency increases and should yield a tighter beam width. Investigating the magnitudes of the filtered results reveals that both the fundamental and the 1st harmonic are approximately equally audible which is undesirable but the fundamental tone is still distinguishable. The 2nd harmonic is hardly audible but still present which is more desirable since it makes it less distinguishable.

Directional audio system development discussion: The development of the directional audio system as a whole explored many facets of engineering and resulted in a functional prototype producing a functional directional audio beam. The resultant output of the system may not be ideal as distortion is prevalent in the system, however; the prototype system manages to prove that a low cost directional audio system is possible. During implementation

it was discovered that the integration of the signal only served to further distort the signal and resulted in the application only square-rooting the signal during pre-processing. This coincides with prior works discussed during the literature review where no integration was performed on the signal despite the presence of the double derivative in Berklay's far-field solution [1] shown in equation 2.

The designs for the system focused quite heavily on the ultrasonic transducer array since there has been little discussion of its design in the prior works found during the literature review. The design process provided helpful insight into selecting an appropriately packed array given the constraints of the project and may be further iterated on in a future implementation of this project. A intriguing investigation into modular transducer array PCBs was explored and discovered little benefit compared to a monolithic design since the output performance of the system was prioritised. A future implementation of this project may revisit this modular approach as scaling up the existing array design to hold more transducers would require new packing simulations and overall redesign of the array.

The auditory experience the system created was unlike any listening experience encountered before. The location of the sound source was clearly evident when transitioning in and out of the radiated beam as far as 4.5m away. As the beam passed from one ear to the next, the audio experienced sharp changes in intensity for each ear while giving the apparent experience that the sound was inside ones own head when the beam was centred on ones face. Additionally, the beam appears to reflect quite well off of non-absorbent surfaces. The resultant reflection maintained its directional effect (while reducing in intensity) and gave the illusion that the reflecting surface was now the source of the sound.

8.2 Conclusion

To conclude, the project successfully achieved the project goal of producing a simple, low-cost prototype of a directional audio system purely to demonstrate the directional audio effect. Each developmental milestone was achieved and produced an output for the next developmental milestone. All these goals were achieved well within budget featuring a cost of under ZAR 1000 mostly due to the use of software for pre-processing of audio. The resultant directional audio system successfully achieves a directional ultrasonic beam which self-demodulates in the environment and creates a directional audio beam as demonstrated by the directivity results. The audio beam suffers from 1st and 2nd harmonic distortion which is undesirable, but could not be corrected within the scope of this project due to time and cost limitations. Furthermore, the distortion tests reveal that the 1st harmonic has a larger presence than the fundamental frequency of the test tone when the beam strikes the microphone head on, however; the fundamental frequency is stronger than the harmonics when the beam is off centre of the microphone. This was suspected to be an issue relating to the large carrier AM used by the mixer. The apparent directionality of the system to human

hearing subjectively appears highly directional due to the stereo hearing capability of human hearing. The source of the sound is easily identifiable when in the beam and less so when outside of it. This beam was easily heard at distances up to 4.5m away with little widening of the beam. The audio beam also appeared to be able to reflect off non-absorbent surfaces and maintaining its directionality, resulting in the surface appearing as the sound source. The project as a whole could be further improved on as it was heavily restrained in scope due to the Covid-19 pandemic of 2020. The project was initially planned out over the course of the semester as shown in appendix B, however; the national lockdown reduced access to many developmental resources offered by UCT and derailed a lot of this planning. This restrained scope results in the project having many avenues for improvement which are discussed in the next subsection.

8.3 Future improvements

The directional audio system produced an effective proof of concept demonstrating the directional audio effect. Unfortunately the resultant audio suffered from significant 1st and 2nd harmonic distortion which is undesirable in a directional loudspeaker. A future implementation of this system could explore alternative modulation techniques and identify which technique results in a lowered cost implementation with a higher quality audio beam.

Another facet of research includes the characterisation of the transducers for use in simulation. The frequency response and transfer function of the transducer could be measured and imported into simulations, allowing for a more realistic signal simulation of the entire signal chain. This could help in discovering what modulation and pre-processing techniques work best with the limited bandwidth of the transducers in use.

The transducer array designed in this project produced a relatively strong directivity compared to a traditional speaker but struggled to produce significant sound pressure levels. A future improvement could investigate alternative transducers or even larger scale transducer arrays and how they effect the resultant output power of the system. This improvement may want to investigate the use of alternatively shaped modular PCBs for the array as the solution in this project is not easily scalable.

Finally, due to challenges external to the project; resources for testing were limited. Ideally the incident angle of the beam relative to the microphone would have produced far more intuitive test results than what was shown in this report. A future implementation may want to consider placing the array on a platform with remotely controllable rotation increments. Then capturing recordings at set angles relative to the microphone and processing this into a beam pattern plot for a more conventional directivity result.

9 References

- [1] H. Berkay, “Possible exploitation of non-linear acoustics in underwater transmitting applications,” *Journal of Sound and Vibration*, vol. 2, no. 4, p. 435–461, 1965.
- [2] P. J. Westervelt, “Parametric acoustic array,” *The Journal of the Acoustical Society of America*, vol. 35, no. 4, p. 535–537, 1963.
- [3] M. B. Bennett and D. T. Blackstock, “Parametric array in air,” *The Journal of the Acoustical Society of America*, vol. 57, no. 3, p. 562–568, 1975.
- [4] M. Yoneyama, J. Fujimoto, Y. Kawamo, and S. Sasabe, “The audio spotlight: An application of nonlinear interaction of sound waves to a new type of loudspeaker design,” *The Journal of the Acoustical Society of America*, vol. 73, no. 5, p. 1532–1536, 1983.
- [5] T. D. Kite, J. T. Post, and M. F. Hamilton, “Parametric array in air: Distortion reduction by preprocessing,” *The Journal of the Acoustical Society of America*, vol. 103, no. 5, p. 2871–2871, 1998.
- [6] F. J. Pompei, “Sound from ultrasound: The parametric array as an audible sound source,” Ph.D. dissertation, Massachusetts Institute of Technology, 2002.
- [7] E.-L. Tan, P. Ji, and W.-S. Gan, “On preprocessing techniques for bandlimited parametric loudspeakers,” *Applied Acoustics*, vol. 71, no. 5, pp. 486–492, 2010.
- [8] W.-S. Gan, J. Yang, and T. Kamakura, “A review of parametric acoustic array in air,” *Applied Acoustics*, vol. 73, no. 12, pp. 1211–1219, 2012.
- [9] F. Farias and W. Abdulla, “A method for selecting a proper modulation technique for the parametric acoustic array,” *Journal of Physics: Conference Series*, vol. 1075, p. 1–6, 2018. [Online]. Available: <https://iopscience.iop.org/article/10.1088/1742-6596/1075/1/012035/pdf>
- [10] J. P. Holosonics Research Labs, “Focused audio technology,” Aug 2002. [Online]. Available: <https://www.holosonics.com/>
- [11] J. Bezanson, A. Edelman, S. Karpinski, and V. B. Shah, “Julia: A fresh approach to numerical computing,” *SIAM review*, vol. 59, no. 1, pp. 65–98, 2017. [Online]. Available: <https://doi.org/10.1137/141000671>
- [12] D. Padua, *FFTW*. Boston, MA: Springer US, 2011, pp. 671–671. [Online]. Available: https://doi.org/10.1007/978-0-387-09766-4_397

- [13] W. Alpha, “Alpha examples: Geometric packing in 2d,” Apr 2018. [Online]. Available: <https://www.wolframalpha.com/examples/mathematics/geometry/packing-and-covering-problems/geometric-packing-in-2d/>
- [14] A. J. Wilkinson, “Eee3055f lecture notes,” 2017.
- [15] S. Russell, “Juliaaudio/portaudio.jl,” 2016. [Online]. Available: <https://github.com/JuliaAudio/PortAudio.jl>

Appendix A Audio pre-processing code

The following code records, processes and then plays the double integrated and square-rooted output. Additional code sources are available on the github repository for this project at https://github.com/SnoWHandS/Directional_Audio_System.

Listing 8: Record, process and play Julia code

```
#Developed by Dillon Heald for use with a directional ultrasonic speaker array
#Date: April 2020

using PortAudio, Statistics, PyPlot, FFTW

stream = PortAudioStream(1, 1, blocksize=1024)

offset = 20

A = 1750                      #Amplitude multiple for final output signal
sample_rate = 44100
Nseconds = 10
N = Nseconds * sample_rate
Δt=1/sample_rate               #seconds: inverse of sample rate
t=(0:N-1)*Δt                  #time axis def
#Define f_axis
Δf=1/(N*Δt)
f=0:(N-1)*Δf
#create array of freq values stored in f_axis. First element maps to 0Hz
if mod(N,2)==0      # case N even
    f_axis = (-N/2:N/2-1)*Δf;
else    # case N odd
    f_axis = (-(N-1)/2 : (N-1)/2)*Δf;
end

#Function for integrating a signal via Riemann sums
function integrate(x, Δt)
    N=length(x)
    y=zeros(N);
    for n=2:N
        y[n]=x[n-1]*Δt + y[n-1]
    end
    return y
end

#Function for high pass filtering a time domain
function hpf(in_signal, time_step, cutoff_freq)
    out_signal = Array{Float64}(undef, length(in_signal));
    RC = 1/(2*pi*cutoff_freq);
    a = RC/(RC + time_step);
    out_signal[1] = in_signal[1]
    for i = 2:length(in_signal)
```

```

        out_signal[i] = a*(out_signal[i-1] + in_signal[i] - in_signal[i-1]);
    end;
    return out_signal;
end;

println("Recording $(Nseconds) seconds of sampled audio")

buf_read = read(stream,N)
buf = buf_read

println("Processing $(Nseconds) seconds of sampled audio")

#Shift function to above 0 for preprocessing
buf = buf_read

#integrate once with function centered at 0
y1 = integrate(buf, Δt)
Y1 = fft(y1)
y1_filt = hpf(y1,Δt,80)
Y1_filt = fft(y1_filt)
#integrate twice
y2 = integrate(y1_filt, Δt)
Y2 = fft(y2)
y2 = hpf(y2,Δt,160)
y2_filt = hpf(y2,Δt,160)
Y2_filt = fft(y2_filt)

#Shift function to above 0 for preprocessing
buf = y2_filt.-minimum(y2_filt)

#Perform a square root of the samples
buf = sqrt.(buf)

close("all")
figure(2)
nStart=Int(round(Δt/Δt))
nEnd=Int(round(N*Δt/Δt))
subplot(3,1,1)
plot(t[nStart:nEnd],y1_filt[nStart:nEnd])
xlabel("y1 output")
subplot(3,1,2)
plot(f_axis,abs.(fftshift(Y1)))
xlabel("FFT of Y1")
subplot(3,1,3)
plot(f_axis,abs.(fftshift(Y1_filt)))
xlabel("FFT of Y1 filtered")

figure(3)
nStart=Int(round(Δt/Δt))
nEnd=Int(round(N*Δt/Δt))
subplot(3,1,1)
plot(t[nStart:nEnd],y2_filt[nStart:nEnd])
xlabel("y2 output")
subplot(3,1,2)
plot(f_axis,abs.(fftshift(Y2)))

```

```

xlabel("FFT of Y2")
subplot(3,1,3)
plot(f_axis,abs.(fftshift(Y2_filt)))
xlabel("FFT of Y2 filtered")

#filter away DC
buf = hpf(buf,Δt,75)

#shift center back to 0 and amplify to be audible
buf = A*buf

BUF = fft(buf)
BUF_READ = fft(buf_read)

figure(1)
nStart=Int(round(0.0025/Δt))           #Artifact with samples before 0.0025s = 2.5ms
nEnd=Int(round(N*Δt/Δt))
subplot(4,1,1)
plot(t[nStart:nEnd],buf[nStart:nEnd])
xlabel("envelope output")
subplot(4,1,2)
plot(t[nStart:nEnd],buf_read[nStart:nEnd])
xlabel("original output")
subplot(4,1,3)
plot(f_axis,abs.(fftshift(BUF_READ)))
xlabel("FFT of original")
subplot(4,1,4)
plot(f_axis,abs.(fftshift(BUF)))
xlabel("FFT of output")

println("Playing $(Nseconds) seconds of sampled audio")

write(stream, buf)
close(stream)

```

Appendix B Project management & planning

The following project planning was performed following initial proposal of the project. By mid March, the Covid-19 pandemic struck South Africa and resulted in national lock down. This altered the scope of the project and shifted timelines, thus the date information is not accurate; however, the work flows remained the same albeit shifted and reduced in scope to account for the disruption.

B.1 Work breakdown structure

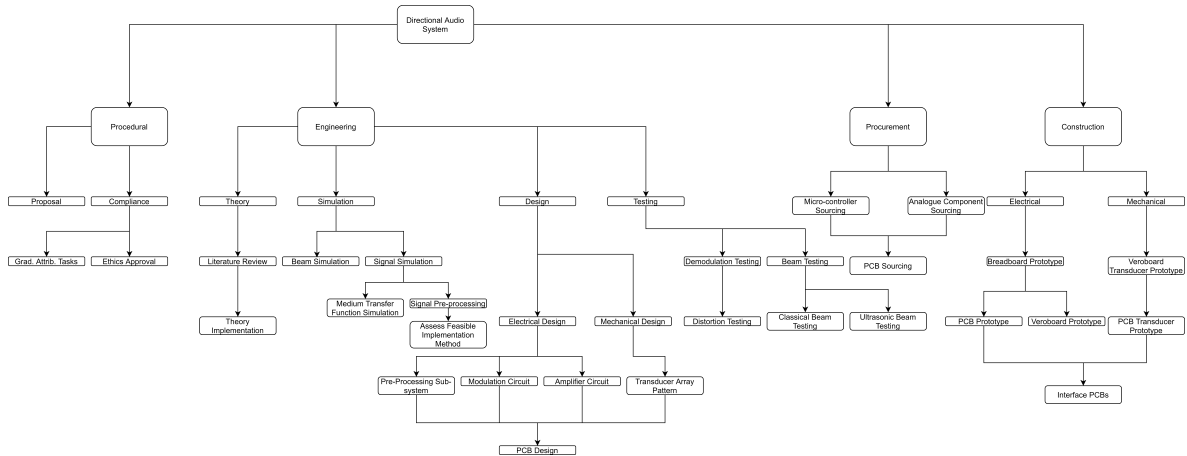


Figure B.1: Work breakdown structure for the the directional audio system

B.2 Gantt chart

| ① | Name | Duration | Start | Finish | Predecessor | Feb 17 - Feb 23 '20 | | | | | | | Feb 24 - Mar 1 '20 | | | | | | | Mar 2 - Mar 8 '20 | | | | | | | Mar 9 - Mar 15 '20 | | | | | | | |
|----|------------------------------------------|----------|------------|------------|-------------|---------------------|---|---|---|---|---|---|--------------------|---|---|---|---|---|---|-------------------|---|---|---|---|---|---|--------------------|---|---|---|---|---|---|--|
| | | | | | | M | T | W | T | F | S | S | M | T | W | T | F | S | S | M | T | W | T | F | S | S | M | T | W | T | F | S | S | |
| 1 | Literature Review | 5days | 24/02/2020 | 28/02/2020 | | | | | | | | | | | | | | | | | | | | | | | | | | | | | | |
| 2 | Beam Simulation | 12days | 24/02/2020 | 10/03/2020 | | | | | | | | | | | | | | | | | | | | | | | | | | | | | | |
| 3 | Signal Pre-processing Simulation | 7days | 24/02/2020 | 03/03/2020 | | | | | | | | | | | | | | | | | | | | | | | | | | | | | | |
| 4 | Medium transfer Function Simulation | 6days | 04/03/2020 | 11/03/2020 | 3 | | | | | | | | | | | | | | | | | | | | | | | | | | | | | |
| 5 | Pre-Processing Sub-System | 12days | 04/03/2020 | 19/03/2020 | 3 | | | | | | | | | | | | | | | | | | | | | | | | | | | | | |
| 6 | Modulation Circuit | 12days | 24/02/2020 | 10/03/2020 | | | | | | | | | | | | | | | | | | | | | | | | | | | | | | |
| 7 | Amplifier Circuit | 12days | 24/02/2020 | 10/03/2020 | | | | | | | | | | | | | | | | | | | | | | | | | | | | | | |
| 8 | Transducer Array Pattern | 4days | 11/03/2020 | 16/03/2020 | 2 | | | | | | | | | | | | | | | | | | | | | | | | | | | | | |
| 9 | Breadboard prototyping | 7days | 20/03/2020 | 30/03/2020 | 5,6,7 | | | | | | | | | | | | | | | | | | | | | | | | | | | | | |
| 10 | Veroboard Transducer Prototype & Testing | 3days? | 31/03/2020 | 02/04/2020 | 8,9 | | | | | | | | | | | | | | | | | | | | | | | | | | | | | |
| 11 | PCB Design Rev 1 Complete | 4days | 03/04/2020 | 08/04/2020 | 10,9 | | | | | | | | | | | | | | | | | | | | | | | | | | | | | |
| 12 | PCB Sourcing | 14days | 09/04/2020 | 28/04/2020 | 11 | | | | | | | | | | | | | | | | | | | | | | | | | | | | | |
| 13 | Demodulation Testing | 6days | 03/04/2020 | 10/04/2020 | 9,10 | | | | | | | | | | | | | | | | | | | | | | | | | | | | | |
| 14 | Distortion Testing | 5days | 29/04/2020 | 05/05/2020 | 12 | | | | | | | | | | | | | | | | | | | | | | | | | | | | | |
| 15 | Classical Beam Testing | 7days | 09/04/2020 | 17/04/2020 | 11 | | | | | | | | | | | | | | | | | | | | | | | | | | | | | |
| 16 | Ultrasonic Beam Testing | 5days | 29/04/2020 | 05/05/2020 | 12 | | | | | | | | | | | | | | | | | | | | | | | | | | | | | |
| 17 | PCB Design Rev 2 | 15days? | 09/04/2020 | 29/04/2020 | 11 | | | | | | | | | | | | | | | | | | | | | | | | | | | | | |
| 18 | Enclosure Design (Optional) | 5days | 30/04/2020 | 06/05/2020 | 17 | | | | | | | | | | | | | | | | | | | | | | | | | | | | | |
| 19 | Literature Review Essay | 7days? | 02/03/2020 | 10/03/2020 | 1 | | | | | | | | | | | | | | | | | | | | | | | | | | | | | |
| 20 | Simulation Method & Results | 5days? | 12/03/2020 | 18/03/2020 | 2,3,4 | | | | | | | | | | | | | | | | | | | | | | | | | | | | | |
| 21 | Circuit Design | 7days? | 20/03/2020 | 09/03/2020 | 5,6,7 | | | | | | | | | | | | | | | | | | | | | | | | | | | | | |
| 22 | Transducer Array Design | 7days? | 17/03/2020 | 25/03/2020 | 8 | | | | | | | | | | | | | | | | | | | | | | | | | | | | | |
| 23 | PCB Design | 2days | 09/04/2020 | 10/04/2020 | 11 | | | | | | | | | | | | | | | | | | | | | | | | | | | | | |
| 24 | Prototype Testing Method & Results | 7days? | 03/04/2020 | 13/04/2020 | 9,10 | | | | | | | | | | | | | | | | | | | | | | | | | | | | | |
| 25 | Classical Beam Testing Method & Results | 3days | 20/04/2020 | 22/04/2020 | 15 | | | | | | | | | | | | | | | | | | | | | | | | | | | | | |
| 26 | Distortion Testing Method & Results | 2days | 06/05/2020 | 07/05/2020 | 14 | | | | | | | | | | | | | | | | | | | | | | | | | | | | | |
| 27 | Ultrasonic Beam Testing Method & Results | 2days | 06/05/2020 | 07/05/2020 | 16 | | | | | | | | | | | | | | | | | | | | | | | | | | | | | |
| 28 | Finalise Report | 2days? | 08/05/2020 | 11/05/2020 | 27,28 | | | | | | | | | | | | | | | | | | | | | | | | | | | | | |
| 29 | Review Report | 5days? | 12/05/2020 | 18/05/2020 | 28 | | | | | | | | | | | | | | | | | | | | | | | | | | | | | |

Figure B.2: Gantt chart part 1

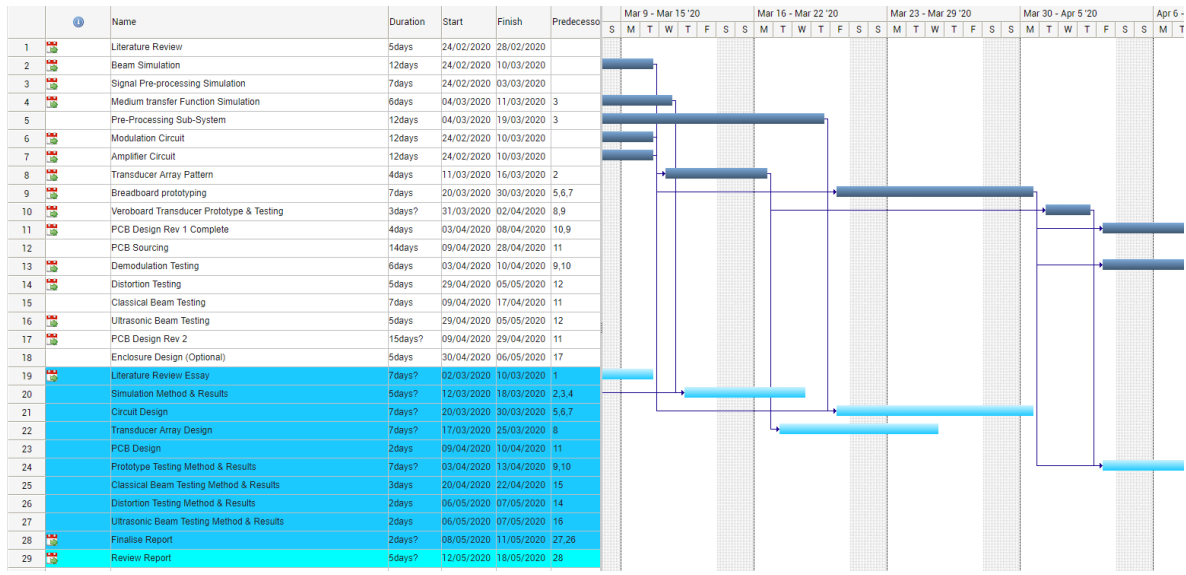


Figure B.3: Gantt chart part 2

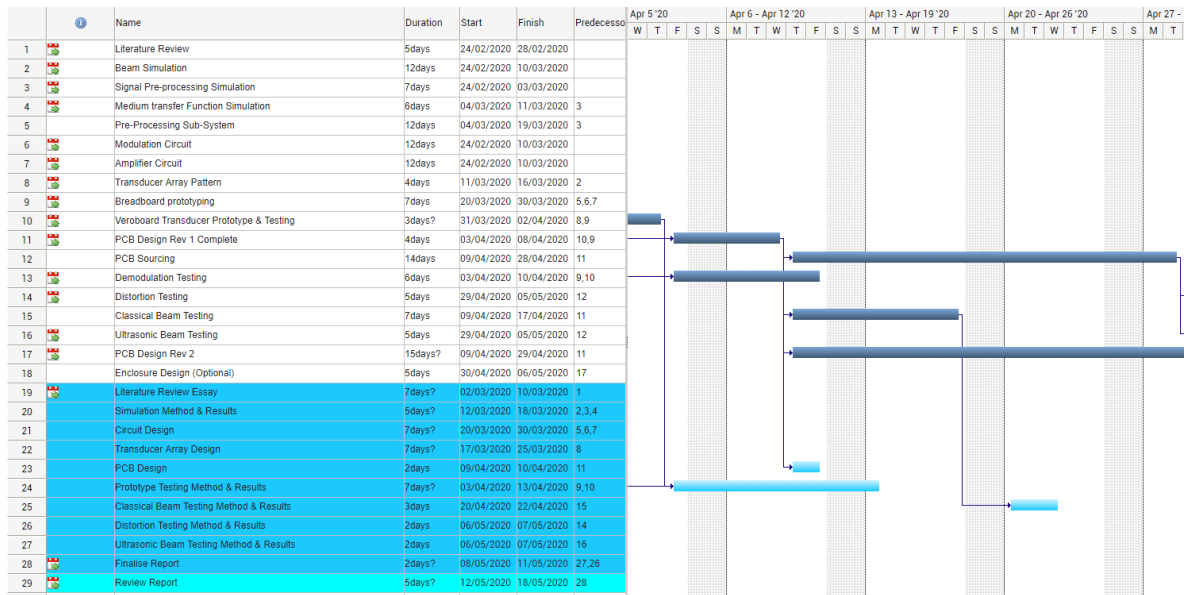


Figure B.4: Gantt chart part 3

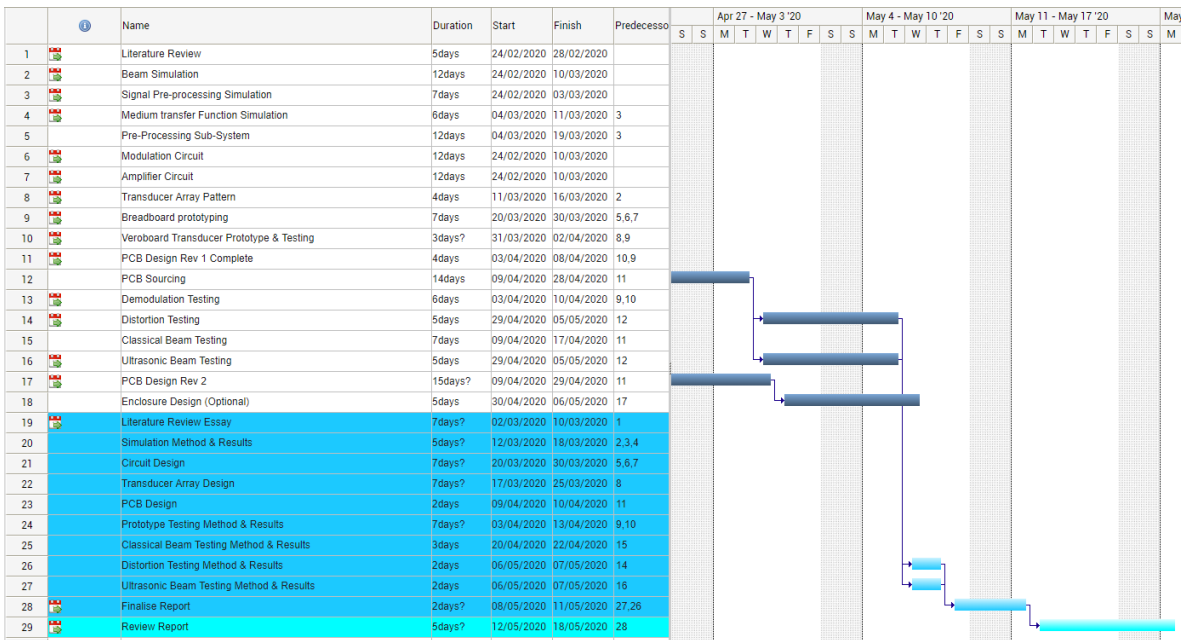


Figure B.5: Gantt chart part 4

Appendix C Beam pattern simulation code

Note, the code used for beam pattern simulation does not translate the ω axis to a θ axis. However, this can be done by performing some of the following changes.

Let Δx be the sample spacing and N be the number of samples. Considering that our sampled DFT array has indices $k=0,1,2..$ where each is the frequency index. In the FFT array, the sample spacing is $\Delta f = \frac{1}{N\Delta x}$.

Since $f = k\Delta f$ with $\Delta f = \frac{1}{N\Delta x}$ the θ axis can be defined by $\theta = \sin^{-1}(k\Delta f \lambda)$. Note however, this is only valid for $|f\lambda| < 1$ or $|f| < \frac{1}{\lambda}$ with angular range $-\frac{\pi}{2} < \theta < \frac{\pi}{2}$ which results in a frequency range of $-\frac{1}{\lambda} < f < \frac{1}{\lambda}$ since the arcsine function outside these bounds will give an error.

The following code shown in listing 9 demonstrates the Julia code used to create the beam shape plots without the above mentioned axis change. This version is for the hexagonally packed array, however; another version of the code for the square packed array is available in the project repository at https://github.com/SnowHandS/Directional_Audio_System.

Listing 9: Beam pattern simulation code for hexagonally packed array

```
# Script to calculate beam pattern from aperture distribution
# 2D FFT Method
# AJW & DH 2020-05-08
#
# To do: relate frequency domain to angle and label plot axes.
using FFTW

# Define a matrix of points to hold the aperture.
dx = 1.0
dy = dx
# Making N bigger implements zero-padding for finer other-domain spacing.
N=1024;
# A holds the aperture distribution (e.g. Sound pressure level or E field strength)
A=zeros(N,N);
x_axis = 0:dx:(N-1)*dx
y_axis = 0:dy:(N-1)*dy

function fill_circle(x0,y0,r0,fill_value,A)
# This function fills a circle, centres (x0,y0) of radius r
# with ones inside matrix A
# Array A is passed by reference
(Ncols,Nrows)=size(A)

i0=x0/dx
j0=y0/dy
iStart=Int(round(i0-(r0/dx+1)))
iEnd=Int(round(i0+(r0/dx+1)))
jStart=Int(round(j0-(r0/dy+1)))
```

```

jEnd=Int(round(j0+(r0/dy+1)))

for i=iStart:iEnd;
    for j=jStart:jEnd
        x = i*dx
        y = j*dy
        R = sqrt( (x-x0)^2 + (y-y0)^2 )
        if R<=r0
            A[i,j]=fill_value
        end
    end
end

function createArray(x1,y1,r1)
    (Ncols,Nrows)=size(A)
    for i=1:Ncols;
        for j=1:Nrows
            x = i*dx
            y = j*dy
            R = sqrt( (x-x1)^2 + (y-y1)^2 )
            if R<=r0
                fill_circle(x0,y0,r0,fill_value,A)
            end
        end
    end
    #define dimensions of the square grid
dimx=7 #2x2 = 18 3x3 = 9 9x9 = 18/8
dimy=7
offset=1.25 #accounts for the external radius of the transducer
# Fill Aperture matrix with one circular object
ApertureDia = 13.7
r0= ApertureDia/2 #interior radius = 13.7/2 = 6.85mm
x0=N/4;
y0=N/4;
fill_value=1;
transducerDia = 16.2

elementSpacing = transducerDia - 0.7
wavelength=(343/40000)*1000; #in mm
# d sin(theta) = lambda -> around 30.3
First_grating_lobe_angle_deg = asin(wavelength;elementSpacing)/pi*180
println("First_grating_lobe_angle_deg = $(First_grating_lobe_angle_deg), deg")

xmid = x0 + (dimx-1)*sqrt(3)*elementSpacing/2
ymid = y0 + (dimy-1)*elementSpacing/2
#array_radius = (xmid-x0) + elementSpacing/2
array_radius = 41
for i=0:dimx-1
    for j=0:dimy-1
        x1 = x0+(i*sqrt(3)*elementSpacing)
        y1 = y0+(j*elementSpacing)
        radial_distance = sqrt((x1-xmid)^2+(y1-ymid)^2)

```

```

        if radial_distance <= array_radius
            fill_circle(x1,y1,r0,fill_value,A)
        else
            #fill_circle(x1,y1,r0,0.25,A)
        end
        x1 = x1 + sqrt(3)*elementSpacing/2
        y1 = y1 + elementSpacing/2
        radial_distance = sqrt((x1-xmid)^2+(y1-ymid)^2)
        if radial_distance <= array_radius
            fill_circle(x1,y1,r0,fill_value,A)
        else
            #fill_circle(x1,y1,r0,0.5,A)
        end
    end
end
#fill_circle(xmid,ymid,r0/2,2,A)

B = fftshift(abs.(fft(A)))    # beam pattern
#close("all")
# PyPlot commands (One can also use Plots with plotly backend)
if(false)
    using PyPlot
    figure(1)
    mycolormap = "jet"  # "hsv" "grey" etc. "jet", "
    imshow(A); colorbar()
    figure(2)
    imshow(B, cmap=mycolormap); colorbar()
    figure(3)
    surf(A, cmap=mycolormap)
    figure(4)
    surf(B, cmap=mycolormap)
    figure(5)
    surf(20*log10.(B .+ maximum(B)/10000), cmap=mycolormap)
end

# Plots commands for plotly() backend - uses OpenGL graphics
if(true)
    using Plots  # takes 60s to first plot, but worth the wait!

    plotly()      # Plot appears in browser window
    #gr()
    #pyplot()

    heatmap(A, size = (1440, 900),reuse=false)
    gui()

    heatmap(B,size = (1440, 900), reuse=false)
    gui()
    surface(A, size = (1440, 900),reuse=false)
    gui()

    surface(B, size = (1440, 900), reuse=false)
    gui()
    #=

```

```
surface(20*log10.(B .+ maximum(B)/10000), color=cgrad(:red,:blue]), reuse=false)
gui()=#
end
```